NASA TECHNICAL MEMORANDUM

NASA TM X 73979

NASA TM X-73979

(NASA-TM-X-73979) THE DESIGN AND FABRICATION OF MICROSTRIP OMNIDIRECTIONAL ARRAY ANTENNAS FOR AEROSPACE APPLICATIONS (NASA) 67 p HC A04/MF A01 CSCL 09A

N77-13332

Unclas G3/33 56945

THE DESIGN AND FABRICATION OF MICROSTRIP OMNIDIRECTIONAL ARRAY ANTENNAS FOR AEROSPACE APPLICATIONS

by

T. G. Campbell, M. W. Appleton, and T. K. Lusby

NASA
National Aeronautics and Space Administration
Langley Research Center
Hampton, Virginia 23665

1. Report No.	2. Government Accession No.	3. Recipient's Catalog No.
NASA TM X-73979		

4. Title and Subtitle	5. Report Date
The Design and Fabrication of Microstrip Omnidirectional Array Antennas for Aerospace Applications	November 1976
	6. Performing Organization Code
7. Author(s)	8. Performing Organization Report No.
T. G. Campbell, M. W. Appleton, and Thomas K. Lusby	
	10. Work Unit No.
9. Performing Organization Name and Address	
NASA Langley Research Center Hampton, VA 23665	11. Contract or Grant No.
	13. Type of Report and Period Covered
12. Sponsoring Agency Name and Address	Technical Memorandum
National Aeronautics & Space Administration Washington, DC 20546	14. Sponsoring Agency Code

15. Supplementary Notes

16. Abstract

A Microstrip Antenna Design Concept has been developed at NASA - Langley Research Center that will provide qusi-omnidirectional radiation pattern characteristics about cylindrical and conical aerospace structures. L-band and S-band antenna arrays were designed, fabricated, and in some cases, flight tested for rocket, satellite, and aircraft drone applications. Each type of array design is discussed along with a thermal cover design that was required for the sounding rocket applications.

17. Key Words (Suggested by Author(s))	18. Distribution Statement
Microstrip antenna; aerospace applications; fabrication	Unclassified - Unlimited

19. Security Classif. (of this report)	20. Security Classif. (of this page)	21. No. of Pages	22. Price*
Unclassified	Unclassified	64	$4.25

*For sale by the National Technical Information Service, Springfield, Virginia 22161

THE DESIGN AND FABRICATION OF MICROSTRIP OMNIDIRECTIONAL ARRAY ANTENNAS FOR AEROSPACE APPLICATIONS

By Thomas G. Campbell, Meredith W. Appleton, and Thomas K. Lusby

SUMMARY

A microstrip antenna design concept has been developed at NASA Langley Research Center that will provide quasi-omnidirectional radiation pattern characteristics about cylindrical and conical aerospace structures.

The microstrip antenna arrays consist of printed-circuit elements that are photo-etched on one side of a copper-clad dielectric laminate material. The thickness of the dielectric materials was 0.16 cm (0.0625 in.) and thereby amenable to conformal mounting about each type of support structure. L-band and S-band antenna arrays have been designed, fabricated, and in some cases, flight tested for rocket, satellite, and aircraft drone applications. Since different types of rocket combinations were to be flown, i.e., Nike-Tomahawk, Cajun, Apache, Orion, it was necessary to design antenna arrays for 16.84 cm (6.63 in.), 22.86 cm (9 in.), 30.48 cm (12 in.), and 35.56 cm (14 in.) in diameter. Several of these configurations have been tested successfully during the sounding rocket flight tests launched from the Wallops Flight Center, Wallops Island, Virginia. A 0.94 meter (37 in.) diameter array has also been fabricated and flown successfully on the Dual Air Density Satellite that was launched in December 1975. A program is presently underway whereby this array design concept will be used on the conical radome of an aircraft drone.

Each type of array design is discussed in this report along with a thermal cover design that was required for the sounding rocket applications.

INTRODUCTION

Microstrip, printed-circuit antennas are becoming increasingly popular in many microwave frequency applications for flight projects. This design concept has been discussed by Watkins [1], Pistolkors [2], Munson [3], Howell [4], and Wolff et al [5], to mention a few. As described by the above, this design concept uses radiating elements that are photo-etched on one side of a copper-clad dielectric laminate material. NASA Langley Research Center has been involved in strip-line and microstrip circuit design since 1967, and during the past 3 years, has provided omnidirectional, S-band microstrip arrays for the sounding rocket program of the Wallops Flight Center. Since different types of rocket combinations are used in this program, i.e., Nike-Tomahawk, Cajun, Apache, Orion, it was necessary to design antenna arrays for 16.84 cm (6.63 in.), 22.86 cm (9 in.), 30.48 cm (12 in.), and 35.56 cm (14 in.) in diameter. Several of these configurations have been tested successfully

during flights launched from Wallops Island, Virginia. In addition to the rocket applications, a 0.94-meter (37-in.) diameter array has been fabricated and flown successfully on the Dual Air Density Satellite that was launched in December 1975. A program is presently underway whereby this array design concept will be used on the conical radome of an aircraft drone. The purpose of this report is to discuss the microstrip array concept as well as to present detailed data on the specific designs mentioned. This work could be helpful in other radio frequency applications. In order to use the microstrip concept in rocket applications, the response of the microstrip element to a thermal environment had to be determined. Therefore, these data and a thermal cover design are also presented in this report.

SYMBOLS

D_m	Missile diameter
E_z	Component of electric field in Z-direction
H_r	Magnetic field component
H_ϕ	Magnetic field component
J_n	Bessel function of first type
K	Length of microstrip element
L_ℓ	Length of laminate
N_e	Number of array elements
N_f	Number of circuit feed points
W	Width of microstrip element
W_c	Width of microstrip conductor feed line
Z_c	Characteristic impedance
h_c	Height of capacitor antenna
r	Radius of microstrip disk
t_c	Thermal cover thickness
$t_{\varepsilon r}$	Laminate thickness
ϵ_r	Dielectric constant
λ_o	Wavelength in a vacuum
$\lambda_{\varepsilon r}$	Wavelength in dielectric
η	Impedance of free space

MICROSTRIP RESONATORS

Resonators are spatial regions that support standing-wave oscillations and a microstrip antenna is a simple resonator. Basically, a microstrip antenna is a modification of the circular diffraction antenna described in reference 2, and the circular diffraction antenna is in turn an extension of the capacitor antenna treatment discussed by Schelkunoff and Friis in reference 6. The circular diffraction antenna is formed by placing a conducting disk of radius, r, at a height $h_c << r$ over a conducting ground plane. A dielectric medium exists between the plates and the dielectric constant can vary depending upon the application and frequency of operation.

The field distribution of the microstrip resonator depends upon the geometrical shape and feed method used. Figure 1 shows standard geometries for microstrip resonators. For the rectangular resonator shown in figure 1(a), standing waves will appear in the Z-direction and as the line width increases, standing waves will appear in the X-direction as well.

When a circular disk resonator is used as shown in figure 1(b), standing waves will appear radially and these waves are reflected at the edge and center of the disk. Depending upon the geometry used, the field distribution can become complex and the task of calculating the eigen (resonant) frequencies of the structure can be difficult. A brief discussion will now be presented on methods used to calculate the eigen frequencies of standard microstrip resonators.

CIRCULAR DISK RESONATORS

A simple analysis solution for the circular disk resonator is presented in reference 4 and this solution exists in the following form:

$$E_z = A\, J_n\,(Kr) \begin{cases} \cos\,(n\phi) \\ \sin\,(n\phi) \end{cases} \tag{1}$$

where J_n is the Bessel function of the first type and K is the wave number, $K = \omega[\mu_o \epsilon_o \epsilon_r]^{1/2}$. The electric field strength is independent of the Z-coordinate and using the E_Z component, the magnetic field components can be determined. These are as follows:

$$H_r = \frac{n}{j\omega\mu_o r} A\, J_n\,(Kr) \begin{cases} \sin\,(n\phi) \\ -\cos\,(n\phi) \end{cases} \tag{2}$$

$$H_\phi = \frac{K}{j\omega\mu_o} A\, J_n'\,(Kr) \begin{cases} \cos\,(n\phi) \\ \sin\,(n\phi) \end{cases} \tag{3}$$

where J_n' is the derivative with respect to its argument (Kr). Since the radial component of the surface current must vanish at the edge of the disk (reference 4), $J_n'(Kr)$ equals zero and these roots are tabulated. Therefore, a simple expression results that can be used to calculate the dominant and higher-order resonances for a circular disk. This expression is as follows:

$$f_r = \frac{C_o X_{nm}}{2\pi r\sqrt{\epsilon_r}} \tag{4}$$

where r is the radius of the disk and for $m = 1$

$$X_{n1} = \begin{cases} 3.831, & n = 0, \quad E_{01} \text{ mode} \\ 1.841, & n = 1, \quad E_{110} \text{ mode} \\ 3.054, & n = 2, \quad E_{210} \text{ mode} \\ 4.201, & n = 3, \quad E_{310} \text{ mode} \end{cases}$$

The E_{110} mode is the dominant mode for this configuration. According to the data presented in reference 4, the accuracy of equation (4) above varies from 1.4 to 9.6 percent. The basic inaccuracies of the analysis are due to the fact that the fringing fields at the edge of the disk are neglected as well as the subsequent radiation. Reference 5 presents a more detailed analysis of the microstrip resonator as leakage fields are considered. Therefore, the analysis in reference 5 can be used if a more precise analysis is desired.

THE RECTANGULAR RESONATOR

In a manner similar to the circular disk, the resonant frequencies for the rectangular resonator can be determined. Again, a simple analysis considers only the electromagnetic fields under the sheet and the leakage or fringing fields are neglected. As discussed in reference 5, a tangential magnetic field strength cannot exist in the magnetic wall and only oscillation modes independent of the height coordinate can be excited in a substrate material. As before, the electric field strength of the principle field is assumed to be under the rectangular sheet and is described by:

$$E_y = A \cos\left(\frac{m\pi x}{W}\right) \cos\left(\frac{n\pi z}{L}\right) \tag{5}$$

The expression for calculating the resonant frequencies for this resonator model is given in reference 5 and is repeated below:

$$f_r = \frac{c_o}{2\sqrt{\varepsilon_r}} \sqrt{(m/w)^2 + (n/L)^2} \quad m,n = 0,1,2... \qquad (6)$$

As in the case of the circular disk, the above expression is approximate and the method of reference 5 would be required for improved accuracy. The accuracy of equation (6) was found to be 6 percent for the TE_{10} mode. Since the design and development work for microstrip antennas usually goes through an empirical verification stage anyway, obtaining an extremely accurate analysis method is usually not required. Therefore, these expressions were used and adjudged adequate for preliminary brassboard models.

The array design that is discussed in this report will use rectangular elements only, but arrays of square or circular geometries can be designed in a similar manner. The element design of the rectangular microstrip resonator will be discussed next.

ELEMENT DESIGN

The rectangular (or square) microstrip resonator is a versatile antenna element that can provide a wide range of electrical performance characteristics. As equation (6) indicates, the resonant frequency of the rectangular element is determined by the width of the strip since $w < L$. When the length is reduced to approach the square configuration, then the resonant frequency is affected by both dimensions. The rectangular microstrip element configuration is shown in figure 1(a). The dimensional effects on the electrical performance of the microstrip resonator have been discussed by several authors, but it was observed that additional experimental data were needed. Therefore, an experimental program was initiated that investigated the effects of changing the length and width of the resonator for a standard substrate thickness of 0.16 cm (0.0625 in.). First, the operating radio frequency for these tests was selected to be S-band (2260 MHz) so that the data could be applied directly to a specific array application.

A rectangular microstrip element was constructed on a 0.16 cm (0.0625 in.) Teflon-fiberglass laminate with a coaxial and microstrip feed point located at the center of the long dimension of the rectangle. The width of the microstrip feed line was selected for a 50-ohm characteristic impedance.

The objective of the first series of tests using the rectangular element was to determine the input impedance and radiation pattern characteristics as a function of the length of the element. The width of the element was set to 0.478 $\lambda\varepsilon r$ (wavelength in the dielectric) which is 4.01 cm (1.58 in.) at F = 2280 MHz. The size of the rectangular element was 30.48 x 4.01 cm (12 in. x 1.58 in.) and the length was reduced in 0.51 cm (0.20 in.) increments. Swept frequency impedance measurements were conducted for each incremental length. A few representative plots are shown in figure 2,

and these results indicate the sensitivity of the input impedance for certain resonat r lengths. The impedance data for each element length are summarized in the VSWR versus $(L/\lambda\varepsilon r)$ plot in figure 3. After studying the impedance trend of figure 3, radiation patterns were measured for the $(L/\lambda\varepsilon r)$ values that produced both high and low VSWR impedance conditions. The $(L/\lambda\varepsilon r)$ values used for the pattern measurements are shown on the VSWR plot of figure 3.

The radiation pattern results are presented in figure 4. As expected, the pattern characteristics are affected by the geometry of the resonator. For $L/\lambda\varepsilon r = .98$, the cross-polarized pattern component increases substantially as a higher-order mode is supported. As $(L/\lambda\varepsilon r)$ increases, the cross-polarized amplitude is reduced and the beamwidth of the principle polarization decreases. At $L/\lambda\varepsilon r = 2.0$, the pattern amplitude of both linear polarizations drops substantially (by about 12 dB). For $(L/\lambda\varepsilon r) = 3.02$, the amplitude of the principle polarization is reduced again and the cross polarization has increased. The on-axis pattern amplitudes were obtained from all the pattern plots and the results are presented in figures 5 and 6. All dimensions of the microstrip element are dependent upon the effective dielectric constant of the laminate material and in this case $\varepsilon_r = 2.48 \pm .04$.

The effect of laminate thickness was determined by measuring the resonant frequency of the rectangular element on several laminate thicknesses. The results are presented in figure 7. Increasing the laminate thickness decreases the resonant frequency and a slight increase in bandwidths was also obtained.

Therefore, it can be seen that all dimensions for the microstrip resonator must be selected properly in order to achieve the desired electrical characteristics. The effect of a thermal cover will be discussed next.

THERMAL COVER DESIGN

Since the use of a thermal cover bonded to a microstrip element directly affects the element dimensions, the discussion of the thermal cover design is presented next in this report. The thermal analysis for the Nike-Tomahawk sounding rocket program indicated that a peak surface temperature of 593°C (1100°F) would be experienced during flight. This analysis also indicated that if a microstrip antenna is mounted on the outside surface of the rocket, a Teflon-fiberglass cover 0.32 cm (0.125 in.) thick would reduce the 593°C (1100°F) to about 204°C (250°F) on the antenna surface. The antenna temperature must be well below the melting temperature, 279°C (535°F), of the high temperature solder used to connect the microstrip feed line to the radio frequency connector. A thermal qualification test plan was prepared that outlined a method of determining the electrical performance of a microstrip element versus temperature. A microstrip test sample was prepared and the electrical properties were measured during a heat pulse closely simulating the flight environment. A 0.32 cm (0.125 in.) thermal cover was

bonded over the microstrip element and a thermocouple was sandwiched between the layers. Thermocouples were also placed on the top layer so that the external and internal temperatures could be monitored and recorded. Several thermal tests were conducted initially so that the control settings for the quartz lamps could be determined in achieving the proper heat pulse. A photograph of the thermal test setup is shown in figure 8. A network analyzer was used to monitor the impedance variations of the antenna element as the temperature changes were made. Separate high and low temperature tests were conducted since setup changes had to be made for each test. The electrical performance test results are presented from ambient to 260°C (500°F) during the high temperature run and from ambient to -100°C (-150°F) for the low temperature case. The low temperature test was conducted for additional information purposes and was not related to the Nike-Tomahawk flight test. The thermal profile predicted for the Nike-Tomahawk flight test is shown in figure 9 along with the measured temperature results. It was extremely difficult to control the quartz lamps so that the temperature profile of the outer surface was simulated exactly. The test did indicate that the 0.32 cm (0.125 in.) dielectric cover would reduce the temperature of the antenna element to about 121°C (250°F). The thermal results using 0.16 cm (0.0625 in.) cover thickness are also presented in figure 9 and it can be seen that the element temperature is reduced to about 226°C (440°F). The phase and VSWR characteristics of the microstrip element were measured during the low and high temperature tests and these results are given in figure 10. The VSWR begins to increase rapidly as the temperature increases beyond 149°C (300°F). The phase angle of the input impedance begins to change immediately as the temperature begins to change. This aspect would be a major concern in phased-array design applications. Basically, the thermal qualification tests did indicate that 0.32 cm (0.125 in.) cover thickness would be sufficient to protect the microstrip antenna during the thermal environment of the Nike-Tomahawk flight program. The next step in the design phase was to determine resonant frequency changes versus dielectric cover thickness.

A single microstrip rectangular element 11.43 x 3.96 cm (4.5 in. x 1.56 in.) was fabricated on a 15.24 x 15.24 cm (6 in. x 6 in.) laminate 0.16 cm (0.0625 in.) thick. The resonant frequency of this element was measured versus cover thickness and the results are shown in figure 11. Since the width of the microstrip element determines the resonant frequency, this dimension can be determined from this curve because $w = 0.484\ \lambda\varepsilon_r$. Therefore, the thickness of the dielectric cover material that is required for thermal insulation must be determined as early as possible in the design and development program.

In addition to the frequency detuning effects of the dielectric cover, variations in the dielectric constant of the material will cause further frequency changes that must be determined. For example, a $\pm$ 2 percent variation in the dielectric constant of the material could cause about 10 MHz variation in the actual resonant frequency of an S-band antenna. Therefore, regardless of the accuracy of the analytical process used in predicting the resonant frequencies of the microstrip resonator, brassboard antenna models must be fabricated and tested to account for all dimensional tolerances. Also, it is important to fabricate antennas and thermal covers from the same lot

of laminate material. The fabricating and bonding process will be discussed later in this report.

MICROSTRIP ARRAY DESIGN APPROACH

A general equation is presented in reference 7 that describes the total far-field pattern for circular arrays of antennas. The pattern fluctuation in the azimuthal plane can be determined for a specific model circumference and number of radiating elements. Basically, an omnidirectional criterion is established that indicates the number of radiating elements needed to produce a specific dB fluctuation in the far-field pattern. Typically, 0.50 wavelength elements are used in circular arrays and these elements can generate many different element patterns depending upon specific design configurations. Usually, the element pattern can be represented by a Fourier cosine series as in reference 7. Therefore, the method described has been used extensively in the past in determining the number of elements, element spacing, and feed points required for a particular circular array application.

When the design of circular arrays using microstrip elements was initiated, however, it was obvious that the general approach in determining the array design parameters would be different due to this particular element configuration. As discussed in the section on microstrip element design, it can be noted that different microstrip configurations would affect the element spacing and feed points required for a particular circular array. The method used by Munson [3] in designing a circular array was reviewed in detail. The Munson method is to provide a continuous microstrip resonator about the structure and the number of feed points connected to this resonator must exceed the body circumference in wavelengths. If the number of feed points is less than the circumference in wavelengths, then higher-order TM modes will be excited. The microstrip array design approach discussed in this report emphasizes the use of discrete microstrip elements instead of a continuous resonator. With this method, it was learned that the number of feed points can be reduced considerably and the subsequent evaluation of the complete circular array is based on the performance characteristics of specific elements instead of merely providing a sufficient number of feed points about a continuous resonator.

The microstrip element impedance and pattern data presented earlier in figures 2 through 5 indicate that for certain element dimensions, the impedance and radiation characteristics vary drastically. For example, when $L/\lambda\varepsilon_r < 1$, the VSWR varies from 2.75 to 5.5, and for $L/\lambda\varepsilon_r \simeq 1.0$, 2.0, and 3.0, the VSWR and pattern characteristics would not be amenable for circular array designs and these values should be avoided. The optimum length for the rectangular microstrip element is $1.5\ \lambda\varepsilon_r$ as the input impedance is matched to 50 ohms. Also, the pattern characteristics are suitable for circular array applications. Actually, it was determined that a center-fed rectangular element with $1.3 < L/\lambda\varepsilon_r < 1.8$ is equivalent to two smaller elements fed simultaneously. Therefore, using $1.5\ \lambda\varepsilon_r$ elements would eliminate about

half the feed points required for the circular array design described in reference 3. The design steps for a specific circular array application are outlined below.

1. Determine the length of microstrip laminate material required for the circular array.

2. Determine element dimensions and spacing.

3. Determine the length of the thermal cover for the array.

4. Determine the width of the array.

Each of the design steps will now be discussed.

Circumference of Microstrip Array

The circumference of the microstrip array must be determined so the dimensions of the laminate material can be accurately cut and fastened to the model substructure. As indicated previously, the thickness of the laminate material is 0.16 cm (0.0625 in.). When the material is wrapped around the cylindrical model, the laminate will be in tension and compression. Therefore, the length of the laminate can be determined from the following expression:

$$L_\ell = \pi(D_m + t_{\varepsilon r})$$

and the length in wavelengths is

$$(L_\ell/\lambda\varepsilon_r) = \pi\frac{(D_m + t_{\varepsilon r}\sqrt{\varepsilon_r})}{\lambda_v}$$

where D_m = missile diameter

t_{ε_r} = laminate thickness

ε_r = dielectric constant of laminate

λ_v = wavelength in a vacuum

Determination Number of Elements

After the circumferential length of the laminate material has been determined, then the number of elements can be determined. The optimum element configuration is $1.3 < L/\lambda\varepsilon_r < 1.8$, so the array configuration was

approached on that basis. From the VSWR standpoint, the $1.5\ \lambda\varepsilon_r$ element is desired since nearly a 50-ohm impedance match is provided. Therefore, the number of elements is determined by dividing the laminate length in wavelengths by 1.5. The number of elements must be 2, 4, 8, 16, 32, and 64, if a parallel feed circuit is to be used. For example, if $N_e = 8.74$, for $D_m = .35$ meters (14 in.), then $(N_f = 8)$, eight elements would be selected to facilitate a parallel feed circuit. The remaining $0.74\ \lambda\varepsilon_r$ would be the spacing between elements, i.e.,

$$S_e = \left(\frac{0.74\lambda\varepsilon_r}{N_e}\right).$$

According to Munson [3], if the $(L_\ell/\lambda\varepsilon_r) = 13.12$ wavelengths, and in order to insure $N_f > (L_\ell/\lambda\varepsilon_r)$ and to facilitate a parallel feed circuit, 16 feed points would probably be selected. Using the discrete $(1.5\ \lambda\varepsilon_r)$ elements, however, only eight feed points would be required and only a slight degradation in the far-field pattern would be expected.

Length of Thermal Cover

As discussed earlier, the thermal cover material is also Teflon-fiberglass, and can vary in thickness depending upon the temperatures expected during flight as well as a suitable bending radius for the material. Usually, the cover thickness is 0.16 cm (0.0625 in.) but in the specific Nike-Tomahawk missile application discussed earlier, the cover thickness was 0.32 cm (0.125 in.). Since the length of the thermal cover must be accurately determined, the following expression is used for that purpose:

$$L_c = \pi[D_m + 2\ t_{\varepsilon r} + t_c]$$

where $t_{\varepsilon r}$ = antenna laminate thickness

t_c = thermal cover thickness

As in the case of the antenna laminate, the thermal cover is in tension and compression as it is wrapped around the cylinder so only one cover thickness is used in this calculation.

Width of the Array Laminate

The width of the array depends upon the width of the elements and the minimum allowable spacing between feed lines of the microstrip circuit. The width of the rectangular microstrip elements are about $0.50\ \lambda\varepsilon_r$.

The width of the array can be minimized to the extent the feed circuit can be reduced in size and complexity. For example purposes, the array width of an eight-element, S-band array for a 35.56 cm (14 in.) diameter missile is 13.34 cm (5.25 in.). The feed circuit design and dimensions will be discussed in the next section.

MICROSTRIP CIRCUIT DESIGN

In many of the microstrip circular array designs, a microstrip circuit is used to feed the elements of the array. In some applications, however, it may be necessary to isolate the feed circuit from the array. Additional thermal protection may be required or possibly the dimensions of the entire assembly may need to be minimized. An example of this design would be a microstrip array fed by a strip-line circuit located beneath the array. Microstrip circuits were preferred in the applications presented in this report, so these designs will be discussed.

As indicated previously, a 50-ohm input impedance was desired for the microstrip elements, so the length for the rectangular configuration was set to 1.5 $\lambda\varepsilon_r$. The parameters for the microstrip transmission line were then selected to provide a characteristic impedance of 50 ohms. Design curves for microstrip applications are well known and the curves in reference 8 were used for that purpose. From these curves, the line widths can be determined for a particular laminate thickness, dielectric constant, etc. Since the standard thickness of 0.16 cm (0.0625 in.) is very conducive to conformal mounting, that thickness was used for the circuit design. As the design curves in reference 8 indicate, slight changes in the dielectric constant of the material will cause significant impedance variations. Therefore, microstrip lines of varying widths were fabricated on the 0.16 cm (0.0625 in.) laminate material to determine the effect material and dimensional tolerances would have on the impedance of each line. The line impedances were measured using a time domain reflectometer. Since a thermal cover would be required in some applications, the effect of the cover on line impedance was also determined. The measurement results with and without the thermal cover are presented in figure 12, along with the calculated impedance for the no-cover case. The following equation from reference 9 can be used to calculate line impedance when the extrapolation of design curves becomes difficult:

$$Z_c = \frac{\eta\, t\varepsilon_r}{W_c\sqrt{\varepsilon_r}} \left\{ 1 + \left[1.735\varepsilon_r^{-.0824} \left(\frac{W_c}{t_{\varepsilon v}} \right)^{-0.836} \right] \right\}$$

It can be seen in figure 12 that very good agreement was obtained with the experimental results. From these data, the line widths required for $Z_c = 50$ were found to be 0.43 cm (0.170 in.) and 0.42 cm (0.165 in.) for the no-cover and cover cases, respectively. The line widths for quarter-wavelength transformers were also determined from these data.

Since a feed circuit for an array is composed of many single and coupled lines, it is necessary to determine the operating characteristics of these lines. Essentially, the insertion loss and phase characteristics of a line will depend upon the proximity to other lines and the even or odd mode impedances involved, i.e., the direction of current flow for each line. Therefore, experimental tests were conducted to determine these effects. First, a test was conducted to determine the attenuation, phase, and isolation of two independent 50-ohm microstrip lines. The results are tabulated below (laminate thickness 0.16 cm (0.0625 in.):

Line Spacing $\lambda\varepsilon_r$	Phase	Attenuation	Isolation
∞	0°	.72 dB	-
.45	-.4°	.80 dB	19 dB
.30	+1.2°	1.4	8 dB
.25	-2.0°	3.0	4.4 dB

Therefore, it can be seen that in order to prevent coupling between independent lines, the spacing should be $S_\ell > 0.50\ \lambda\varepsilon_r$. For the case where two lines of the same circuit loop are adjacent, having current flowing in opposite directions, then the line loss and phase will be affected. The following table shows the results of that experimental measurement (laminate thickness 0.16 cm (0.0625 in.).

Line Spacing $\lambda\varepsilon_r$	Phase	Attenuation, dB
.33	0°	.9
.27	-2°	.9
.23	-2°	.8
.21	-1°	.81
.20	+4	.84
.14	+10°	1.6
.11	+26°	3.0

In order to achieve isolation and minimize losses between microstrip lines, the lines should be no closer than .20 $\lambda\varepsilon_r$. The insertion loss measured for a single straight section of 50-ohm microstrip line 0.43 cm (0.17 in.) wide on a 0.16 cm (0.0625 in.) laminate with $\varepsilon_r = 2.48$ was .94 dB/meter (0.286 dB/ft.). A 0.16 cm (0.0625 in.) dielectric cover increased the loss to 1.29 dB/meter (0.391 dB/ft.). These losses were adjudged typical for the dielectric and conductor losses that could be expected for this microstrip configuration. A two-way power divider was fabricated and tested using 0.44 cm (0.175 in.) line widths and line spacings of 1.91 cm (0.75 in.) ($\lambda\varepsilon_r$ = .21 @ 2280 MHz). These lines matched the 50-ohm input impedance of the rectangular element and quarter-wavelength transformers (.33 x 2.24 cm) (.130 x .88 in.)

were used to raise the element impedance to 100 ohms before the two elements were connected together. After connecting the power divider to two elements, a VSWR of 1.05 was measured at the test frequency of 2280 MHz. Later, a complete power distribution circuit was fabricated and tested. Microstrip-to-coaxial fittings were used at the antenna element feed points and they were terminated with 50-ohm impedances as insertion loss measurements were conducted. A 7.1 dB insertion loss was measured for a four-way power split at a frequency of 2280 MHz. This feed circuit arrangement was adjudged acceptable for a complete array design. Therefore, it can be seen that the circuit design, line spacing, etc., can certainly influence the insertion loss characteristics of coupled microstrip transmission lines. So, reducing the width of the array, or placing the feed lines closer together must be carefully considered before completing the final design. The particular circuit dimensions can be noted in the design drawings for the specific circular array design. These are presented later in the report.

MICROSTRIP ANTENNA FABRICATION

The antenna, whether fabricated in one piece or several individual units that constitute a complete array, is etched from 0.16 cm (0.16 in.) thick, double-sided, 56.70 grams (2 oz.), copper-clad laminates of the Teflon-fiberglass type. This technique, however, is applicable to other antenna configurations (i.e., flat plate, circular, etc.) that may be fabricated from a variety of similar copper-clad laminates.

The design requirements for this type of antenna dictate extremely close tolerances in the photo-etching process, necessitating rigid control and inspection at every step of its fabrication. Typical tolerances are $\pm$ .0076 cm (.003 in.) for element size and spacing, and $\pm$ .01 cm (.005 in.) for transmission line and transformer dimensions. In the development of fabrication procedures, a goal was established to meet overall dimensional requirements within a tolerance of $\pm$ .005 cm (.002 in.). This goal is being realized with a fair degree of consistency on antenna units as large as 14.61 cm x 111.76 cm (5.75 in. x 44 in.), with the capability for producing even larger arrays. The fabrication process contains eight categories of effort and these will now be discussed.

Art Work Generation

No photo-etching process can be better than the art work from which the photo resist is exposed, therefore, particular emphasis is placed on accuracy in this area. As shown in figure 13, the art work is generated on Stabilene film at full scale by use of a manually-operated coordinagraph incorporating a precision cutting blade. The Stabilene has a .002 cm (.001 in.) thick opaque film layer on a .01 cm (.004 in.) transparent stable film base. The opaque layer of the Stabilene film, when cut to the proper geometry, can be peeled away to produce either a positive or negative, actual or mirror image representation of the required antenna circuit. In this particular case,

the negative mirror image configuration is used. The coordinagraph has the capability to make the required cuts with an accuracy of ± .002 cm (.001 in.), which can produce an accumulative geometric error of ± .005 cm (.002 in.). The completed art work is checked on a Cordax measuring instrument using optical scanning to insure that it conforms to the design dimensions with a tolerance no greater than ± .005 cm (.002 in.).

Laminate Cleaning

The surface of the copper-clad laminate must be extremely smooth and free of dirt, oils, oxides, and other contaminants to insure proper adhesion of the photo resist and to achieve the necessary resolution in the photo development step. There are several methods of cleaning the laminates, some of which include degreasing with trichlorethylene vapor, scrubbing with pumice slurry, washing in mild HCL solution, rinsing in deionized water, and oven drying. Experience has shown that a scrubber-deburring machine performs this function in a fast and efficient manner, producing a laminate that has been rinsed and dried, and is ready for the photo resist application.

Photo Resist Application

A dry film photo polymer resist is used for its ability to be applied in continuous lengths and to produce good etching results in either acid or alkaline etch solutions. The resist is applied simultaneously to both sides of the cleaned copper-clad laminate by use of a laminator operating at 115°C ± 4° (240°F ± 5°). The photopolymer resist, as supplied, is sandwiched between two thin polyethylene cover sheets. During resist lamination, the cover sheet nearest the copper-clad laminate is automatically peeled away to allow the resist to adhere to the copper surface, while the outer cover sheet is left in place to protect the resist during handling and exposing. After photo resist application, the laminate is allowed to normalize at room temperature for 15 minutes prior to exposure and development. Application of the photo resist, and all subsequent steps through development, must be performed in a gold light environment to prevent unwanted exposure by ambient untraviolet radiation.

Photo Resist Exposure

To achieve the necessary fine line resolution in photo resist exposure, the opaque film side of the photo mask (Stabilene film art work) must be held in intimate contact with the polyethylene cover sheet of the applied photo resist. Light diffusion through a .005 - .007 cm (.002 - .003 in.) space between mask and photo resist can produce an etching error of .010 - .040 cm (.005 - .015 in.). This required intimate contact is accomplished with a 1.21 x 1.52 meter (48 in. x 60 in.) vacuum frame copy board. This setup is shown in figure 14.

Exposure time for proper polymerization of the photo resist is a function of the type and intensity of the exposure system used, and is determined empirically for individual systems. Optimum exposure for the type of resist being used is produced with an indication of 8 to 10 on a Stouffer 21-step sensitivity guide. Best results have been achieved with a 2-minute exposure using three Spectramatic 6000 quartz line lights, operated at 3200°K, located 25.4 cm (10 in.) from the photo mask and spaced equidistant along the antenna length. Since the backside of the antenna retains its copper foil, it is exposed completely without benefit of a mask.

Photo Resist Development

After exposure, the protective polyethylene film is peeled from the resist and the complete antenna unit is developed in a spray developer as shown in figure 15. Developing time is a function of solution temperature, spray distribution and pressure, and the concentration of dissolved resist in the developing solution. The spray developer is operated at 26°C (80°F) and the antenna laminate is oscillated slowly to eliminate concentrated spray jets on any given area. Proper development is determined by visual observation. Optimum developing time is approximately 150 percent of the time required to observe complete loss of color of the unexposed areas of resist. Since the photo resist is developed in an aqueous solution, the work can proceed directly to the etching process.

Chemical Etching

Etching of the radiation elements, transmission lines, and transformers in the copper foil of the laminate is one of the most critical steps in this type of antenna fabrication. The etching (as shown in figure 16) is performed by a conveyor etcher which can handle laminate widths up to 60.96 cm (24 in.) and lengths limited only by the availability of material. The etchant, Shipley Neutra etch V-1, is maintained at a temperature of 43°C (110°F and a Ph level of 7.2 to 7.8. Since the etch rate, and ultimately the pattern dimensions, are dependent on etchant temperature and Ph level as well as conveyor speed, several test circuits were etched and measured to determine the exact conveyor speed to be used for the prevailing etchant condition. After etching, the remaining photo resist is removed with a standard stripping solution, and the laminate is passed through the scrubber deburring machine, as shown in figure 17, to insure smooth copper surfaces and edges. The etched laminate is then checked on a cordax to verify conformance to dimensional tolerances. This can be seen in figure 18.

Finishing

All units found to be within dimensional tolerance are visually and optically inspected for other etching imperfections such as pitting, rounded corners, excessive undercut, etc., and are then cut to size and gold plated as required. A .020-.050 mil thickness of gold plating is electro-deposited

on the back side of the copper foil to prevent oxidation. If the face of the antenna unit is to be exposed without a bonded shield, it is also gold plated for the same reason. Gold plating is accomplished by the brushing action of an absorbent pad (anode) saturated with Selectron SPS 535 solution, power by a Selectron 6035 power pack whose cathode is attached to the copper foil with a clip, as shown in figure 19. The thickness of the electro-deposited gold is calculated from time, current density, surface area, and a constant which is a function of the particular plating solution used. After gold plating, the now complete antenna unit, is rinsed for 5 minutes in D.I. water and dried.

All of the fabrication processes, procedures, techniques, and quality assurance steps outlined above were developed or adapted to insure finished antenna units will meet or exceed design requirements. The final acceptance or rejection of an individual unit, however, must be determined through subsequent radiation pattern and impedance testing. If the electrical tests are successful, with regard to resonant frequency, etc., then the array is scheduled for the application of the thermal cover.

Bonding of Thermal Cover

In figure 20, the antenna and the 0.16 cm (0.0625 in.) thermal cover are being prepared for bonding. In the case of the 0.32 cm (0.125 in.) thermal cover, two separate 0.0625 in. layers were used and bonded separately about the circular array. The HX-1000 bonding film is being placed on the thermal cover and antenna, and then the entire assembly is placed in a cylindrical metal press and clamped together as shown in figure 21. After clamping, the assembly is placed into an oven which is preheated to 218°C (425°F). The mold pressure was at least 7.02 Kgs/cm^2 (100 psi). The bonding parameters of temperature, pressure, and time may be adjusted to meet specific conditions. Bonding in this manner should produce a bond strength (peel) in excess of 3.59 Kg/cm width. In order to improve the temperature control of the oven during the bonding process, it was necessary to place a thermocouple between laminate layers and place that assembly inside the oven as well. This thermocouple indicated that the bond line temperature and the oven heat were controlled accordingly. Bonding the thermal cover in this manner produced adequate bonds but extreme care must be exercised during the bonding process so that delamination does not occur around the edges of the antenna. The physical properties of the laminate material and bonding films are tabulated below:

Typical Properties of HX-1000

Thickness	.003 cm (0.0015 in.)
Water Absorption	0.005 percent
Tensile Strength	4.92 x 10^6 Kgs/sq. meter
Thermal Conductivity	5 x 10^{-4} (cgs)
Dielectric Constant	2.35
Dissipation at X-band	2.5 x 10^{-3}
Bonding Temperature	218°C (425°F)

Typical Properties of Microstrip Laminate Material

Dielectric Constant at 10 GHz	2.48 $\pm$ .04
Flexural Strength (psi)	
Lengthwise	1124.8 Kgs/sq. cm (16,000)
Crosswise	843.6 Kgs/sq. cm (12,000)
Tensile Strength (psi)	
Lengthwise	1406.0 Kgs/sq. cm (20,000)
Crosswise	1124.8 Kgs/sq. cm (16,000)
Coefficient of Thermal Expansion	1.85 x 10^{-5}/°C

In addition to bonding material, the thermal cover is held in place by 100° counter-sunk screws. These screws are also used to attach the antenna to the missile substructure. A template was used to aline the mounting screws as well as to trim the antenna laminate to the exact circumferential length. This effort minimized the gap at the ends of the array. A photograph of the completed antenna is shown in figure 22.

EXPERIMENTAL RESULTS

The microstrip antenna design concept and fabrication method discussed in this report have been used in three specific circular array applications. These applications are presented in this report and they are as listed below:

1. Sounding rocket applications 16.84 cm, 22.86 cm, 30.48 cm, and 35.56 cm (6.63 in., 9 in., 12 in., and 14 in.) in diameter
2. Dual Air Density Satellite (.94 meter diameter)
3. Aircraft drone applications (conical radome application)

The design and experimental data for each of these applications will now be presented.

Sounding Rocket Design

Microstrip circular arrays were designed to provide quasi-omnidirectional radiation patterns about missiles having the following diameters: 16.84 cm (6.63 in.), 22.86 cm (9.0 in.), 30.48 cm (12.0 in.), and 35.56 cm (14.0 in.). The frequency of operation for these antennas is in the 2250 - 2270 MHz range. The maximum heating rate was predicted to occur for the 22.86 cm (9.0 in.) diameter missile so a thermal cover of 0.32 cm (0.125 in.) was required to cover the circular array for that model. Otherwise, a single layer, 0.16 cm (0.0625 in.) was adequate thermal protection for the remaining diameters.

Rectangular ($1.5\ \lambda\varepsilon_r$ x $.478\ \lambda\varepsilon_r$) microstrip elements were used for all of the sounding rocket applications, but in some of the cases, a reduced element length had to be used. The layout for each circular array is shown in figure 23, and the specific dimensions for each element can be noted. The basic concern in each array design was to arrange as many $1.5\ \lambda\varepsilon_r$ elements

about the circumference as practically possible when a parallel feed circuit is used.

The center frequency desired for each array is 2265 MHz; so the effect of the thermal cover on resonant frequency had to be determined. Typically, a 52 MHz frequency shift would occur when a 0.16 cm (0.0625 in.) layer was placed over the rectangular element, so naturally, the resonant frequency without the cover would be 2317 MHz in order to obtain a 2265 MHz operating frequency. Several circular arrays were fabricated for each missile diameter and the resonant frequencies were measured during separate stages of assembly. These frequency data are tabulated in Table I and the repeatability of the manufacturing process can be noted. Additional electrical performance data are also provided in Table I. Prototype antennas were environmentally tested (vibration and shock) according to the test specifications provided in Appendix A.

Typical impedance and pattern characteristics for each array are presented in figure 24. Photographs of the circular arrays are presented in figure 25 and a photograph of the Nike-Orion missile during launch is shown in figure 26. Several of these circular array antennas have been launched on various sounding rocket combinations from Wallops Flight Center and they all have performed satisfactorily.

Dual Air Density Satellite

A microstrip circular array was also designed, fabricated, and flown on the Dual Air Density Satellite. The array diameter was 0.94 meters (37 in.) and the frequency of operation was 2282.5 MHz. The array consisted of 24 rectangular elements with an element spacing of 0.96 cm (0.375 in.). A photograph of the array is shown in figure 27, mounted to the satellite. In this application, the width of the array could not be greater than 12.70 cm (5.0 in.); therefore, the number of microstrip feed lines had to be reduced. The reduction was achieved by feeding the sub-arrays with coaxial cables instead of microstrip lines. The elements of the array were symmetrically located on the laminate and microstrip lines were placed on both sides of the elements. With this arrangement, a 180° phase shift had to be provided between elements of the sub-arrays so that all elements would be in phase in the far field. The pattern and impedance results of this design are shown in figure 28. It can be seen that a very smooth roll-plane pattern was achieved.

Aircraft Drone

A present application is underway whereby a microstrip circular array is placed around a conical radome of an aircraft drone for L-band operation. The usual procedure for such applications is to place monopole antennas on the fuselage of the drone in order to achieve omni-pattern coverage. Unfortunately, it is a difficult task to minimize pattern nulls with this type of design and changes in aircraft control surfaces can accentuate these nulls

during the flight. In order to improve this situation, a circular microstrip array was designed that could be mounted around the nose tipe radome of the drone. With this design, pattern nulls are produced over narrow angular regions off the nose and tail of the aircraft. Consequently, these nulls exist for a very small percentage of the radiation sphere. Whereas in the other design approach, nulls could occur in many areas about the drone and still be subject to change as the drone configuration changes. A drawing of the drone circular arrays is shown in figure 29 and it can be seen that the element feeds had to be modified in order to accommodate the necessary number of $1.5\ \lambda\varepsilon_r$ elements. The resulting impedance and pattern characteristics are presented in figures 30 and 31, respectively.

CONCLUSION

Microstrip circular array designs for omnidirectional aerospace applications have been discussed in this report. L-band and S-band antenna arrays have been designed, fabricated, and flight tested for rocket, satellite, and drone applications. These antennas were fabricated using a method that is very precise but still amenable to mass production techniques. A thermal cover design was also presented that maintains an antenna temperature of 121°C (250°F) while the external surface temperature is 593°C (1100°F). Each of the circular arrays discussed provides exceptional electrical performance characteristics. These circular array designs can be applied to a wide variety of aerospace antenna applications.

REFERENCES

1. Watkins, J.: Circular Resonant Structure in Microstrip. Electronics Letters, October 16, 1969, Vol. 5, No. 21.

2. Pistolkors, A. A.: Theory of the Circular Diffraction Antenna. Proceedings of the IRE, January 1948, pps. 56-60, Proc. 36.

3. Munson, Robert E.: Conformal Microstrip Antennas and Microstrip Phased Arrays. IEEE Transactions on Antennas and Propagation, January 1974.

4. Howell, John Q.: Microstrip Antennas. IEEE Transactions on Antennas and Propagation, January 1975.

5. Wolff, I.; and Knoppik, N.: Microstrip Disc Resonators. (NASA Technical Translation NASA-TTF-15,889), Archiv fuur Elektronik and Uebertragungstechnik Vol. 28, No. 3, 1974, pps. 101-108, A74-26581.

6. Schelkunoff and Friis: Antenna Theory and Practice. Wiley and Sons, 1952, pps. 545-547.

7. Cockrell, C. R.; and Croswell, W. F.: A General Method for Designing Circular Array Antennas to Obtain Quasi-Omnidirectional Patterns. NASA TN D-4254, December 1967.

8. Saad, T. S.: Microwave Engineers' Handbook. Vol. I, 1971, Horizon House - Microwave, Inc.

9. Mackey, W. R.: Review of Microwave Integrated Circuit Technology. Bendix Technical Journal, Winter 1972/73.

TABLE I

Missile Diameter	f_r (MHz) Before Bonding	Approx. f_r (MHz) After Bonding	VSWR @ 2265 MHz
1. 16.84 cm Units (6.63 inches)			
A			
B	2319	2267	1.40
C	2320	2270	
D	2322	2271	1.45
E			
F	2317	2270	1.49
G	2316	2270	1.49
2. 22.86 cm Units (Thermal Cover Thickness 0.125 inches) (9.0 inches)			
A	2327	2263	1.22
B	2323	2256	1.20
C	2330	2268	1.18
D	2328	2264	1.17
E	2328	2262	1.10
F	2329	2264	1.15
G	2332	2259	1.18
H	2322	2252	1.25
J			
K	2333	2268	1.17
L	2338	2278	1.30
M			
N	2333	2268	1.18
O			
P	2331	2268	1.17
3. 30.48 cm Units (12.0 inches)			
H	2318	2270	1.4
J	2307	2263	1.56
K	2317	2270	1.30
R	2324	2279	1.37

TABLE I (CONT'D)

Missile Diameter	f_r (MHz) Before Bonding	Approx. f_r (MHz) After Bonding	VSWR @ 2265 MHz
4. 35.56 cm Units (14.0 inches)			
A	2303	2255	1.47
B	2308	2251	1.42
C	2323	2273	1.38
D	2317	2265	1.33
E	2317	2265	1.35
F	2317	2265	1.30
G	2324	2275	1.41
H	2317	2265	1.38

APPENDIX A

ENVIRONMENTAL TEST SPECIFICATIONS

FOR

DESIGN QUALIFICATION OF NIKE-APACHE

AND

NIKE-CAJUN SOUNDING ROCKET PAYLOADS AND COMPONENTS
(Abstracted from GSFC Document S-320-SR-2 dated June 20, 1968)

General

It will be the responsibility of the Government to conduct the test specified herein. No test documents or reports will be required of the contractor. It will be the contractor's responsibility to provide units which will operate when exposed to the tests specified. All deviations from the enclosed specification must be stated in the contractor's proposal.

SECTION 1 - NIKE-CAJUN AND NIKE-APACHE

1.1 Applicability

These specifications shall apply to payloads, subsystems, experiments, and components which are to be launched by Nike-Cajun and Nike-Apache sounding rockets.

1.2 Test Sequence

The following testing sequence is recommended. It is noted that four of the tests specified are for payload level only.

1.2.1 Leak Detection
1.2.2 Spin
1.2.3 Temperature and Humidity
1.2.4 Vibration and Shock
1.2.5 Acceleration
1.2.6 Thermal Vacuum

1.3 Leak Detection

1.3.1 Applicability

All payloads or components which operate as a hermetically-sealed unit shall be subject to a leak check.

1.3.2 Time of Performance

An initial leak check shall be performed at the beginning of the test program. It shall be repeated following the temperature test and again following vibration test. It shall be further conducted during the thermal vacuum test.

1.3.3 Measurement

Leak rates shall be measured with a helium mass spectrometer. Table 1-3-1 provides the applicable parameters for both prototype and flight payloads.

TABLE 1-3-1

LEAK DETECTION TEST

Pressure of Sealed Specimen	760 mm Hg (abs)
Proportion of Tracer Gas	10% min
Minimum Chamber Pressure	1×10^{-4} mm Hg
Maximum Leak Rate	1×10^{-6} atm std cc/sec

1.4 Spin

Table 1-4-1 specifies the parameters for conducting spin tests on prototype payloads. No spin tests will be conducted at speeds greater than one-half the payload lateral natural frequency.

TABLE 1-4-1

PAYLOAD SPIN TEST

Spin Rate	732 rpm
Duration	1/2 minute

1.5 Temperature and Humidity

1.5.1 Description

This test phase consists of hot and cold operational tests, hot and cold storage tests, and humidity tests.

1.5.2 Storage Test

These tests shall be run at the levels specified in Table 1-5-1. Electrical performance shall be checked prior to and after testing.

TABLE 1-5-1

PAYLOAD AND COMPONENT STORAGE TESTS

Hot Exposure:	Stabilized Temperature 60°C Duration 6 hours
Cold Exposure:	Stabilized Temperature -30°C Duration 6 hours

1.5.3 Humidity Test

This test shall be run at the levels specified in Table 1-5-2. Electrical performance shall be checked prior to and after testing.

TABLE 1-5-2

PAYLOAD AND COMPONENT HUMIDITY TEST

Stabilized Temperature	30°C
Relative Humidity	95 ± 5% RH
Duration	24 hours

1.5.4 Operational Temperature Test

Operational temperature testing shall be conducted on payloads or components in the following manner.

1.5.4.1 Sequence

The hot test shall precede the cold test.

1.5.4.2 Duration

Both tests shall consist of exposing the payload or component to the temperature extreme for a 6-hour period.

1.5.4.3 Test Levels

High temperature shall be +105°F. Low temperature shall be 0°F.

1.6 Vibration

1.6.1 Sinusoidal Vibration

This test consists of sweeping the 'g' level stipulated in Table 1-6-1 once through each frequency range.

TABLE 1-6-1

SINUSOIDAL VIBRATION - PROTOTYPE

Axis	Freq. Range (Hz)	Level ('g' - 0 to peak)	Sweep Rate (oct./min.)
Thrust	10 - 13	0.5 in. d.a.	2
	13 - 120	4.5	
	120 - 300	10.5	
	300 - 400	15.0	
	400 - 2000	7.5	
Lateral (Both Axes)	7 - 11	0.5 in. d.a.	2
	11 - 40	3.0	
	40 - 120	0.036 in. d.a.	
	120 - 2000	7.5	

1.6.2 Random Vibration

Gaussian random vibration shall be applied to the payload or component while in the launch mode for each axis as specified in Table 1-6-2.

TABLE 1-6-2

RANDOM VIBRATION - PROTOTYPE (ALL AXES)

Frequency Range	20 - 2000 Hz
PSD Level	0.45 g^2/Hz
Acceleration	30.0 g/rms
Duration	20 seconds

1.6.3 Sinusoidal Transient

This test consists of two identical thrust axis exposures to a logarithmically decaying sinusoidal transient. The decay rate shall be such that the third cycle peak is one-half the maximum amplitude peak. The maximum amplitude peaks shall be as follows:

Prototype: 54 'g'
Flight: 36 'g'

Frequency of transient input will be a discrete frequency between 120 and 150 Hz. Flight units will be subject to only one exposure to this transient.

1.6.4 Shock Test (Prototype Payload Only)

The payload shall be subjected to the following shock tests in the thrust axis only.

1.6.4.1 Half sine, 70 G peak, 5 milliseconds duration
1.6.4.2 Terminal sawtooth, 60 G peak, 15 milliseconds duration

1.7 Steady State Acceleration

The acceleration tests are applicable to prototype payloads and components. No requirement is made for flight acceptance testing.

1.7.1 Payload

Acceleration shall be applied in the thrust axis only. The level at the base of the payload shall be 60 G's. The duration of the test shall be 1/2 minute.

1.7.2 Component

The component shall be subjected to an acceleration test of 1/2 minute duration in each of three orthogonal axes of component. The level shall be 1.5 times the maximum level expected during flight due to vehicle thrust and spin. The maximum radius from spin axis to CG of component is 2.84 inches.

TABLE 1-7-1

COMPONENT ACCELERATION

Direction	Component X, Y, and Z axes
Magnitude (g's)	$\sqrt{At^2 + An^2} = 100$ G's
Duration	1/2 minute per axis

1.8 Thermal Vacuum

This test phase evaluates the performance of the test item under combined temperature and vacuum environments.

1.8.1 Temperature Extremes

Temperature extremes are outlined in Table 1-8-1.

TABLE 1-8-1

THERMAL-VACUUM TEMPERATURE EXTREMES

High Temperature Limit	185°F
Low Temperature Limit	0°F

1.8.2 Corona Check

A corona check to insure no significant electrical discharge at vacuum shall be conducted at a vacuum pressure of 1×10^{-4} mm Hg.

1.8.3 High Temperature Vacuum

A high temperature vacuum check shall be performed immediately following the corona check. This test shall be performed at a vacuum pressure of 1×10^{-5} mm of Hg with the payload operating at a minimum of two duty cycles. Temperature shall be stabilized for a 2-hour minimum.

1.8.4 Low Temperature Vacuum

Following the high temperature vacuum test, a low temperature vacuum test shall be performed. The temperature shall be stabilized for a minimum of 2 hours at a vacuum pressure of 1×10^{-5} mm Hg. The payload shall be operated through a minimum of two duty cycles.

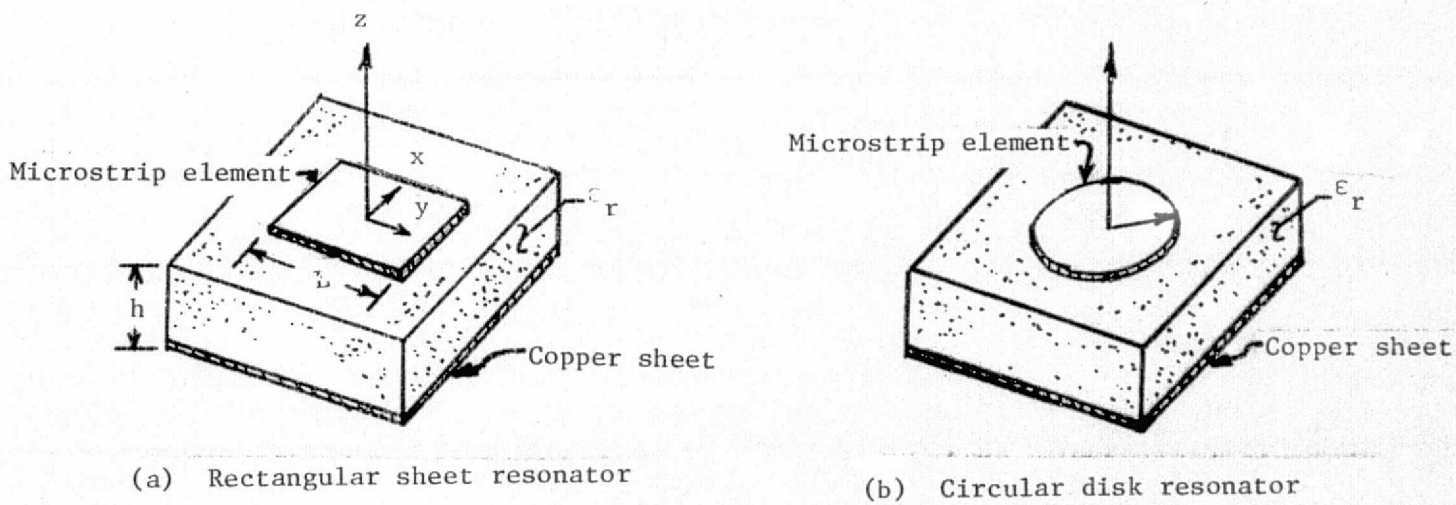

(a) Rectangular sheet resonator

(b) Circular disk resonator

Figure 1. - Rectangular and circular microstrip resonators.

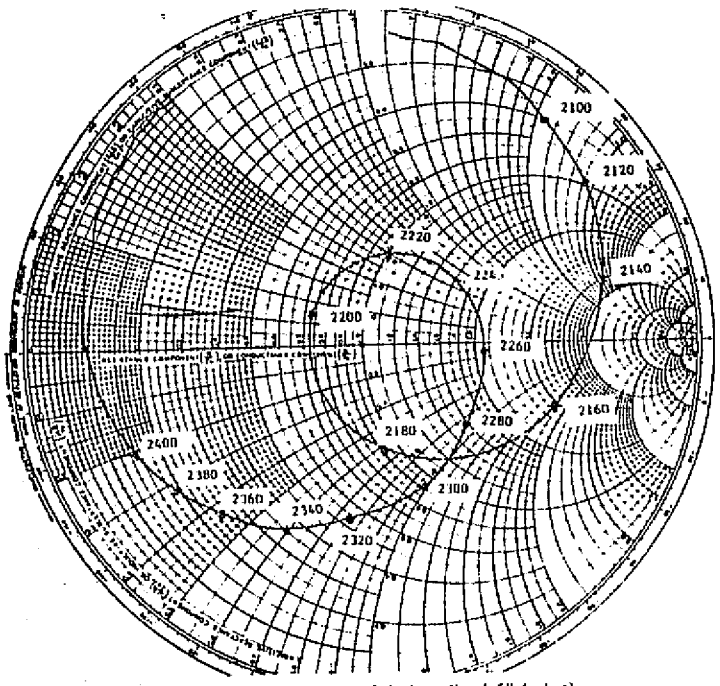

(e) $L/\lambda\varepsilon_r$ = 1.05 (L = 3.5 inches, W = 1.58 inches)

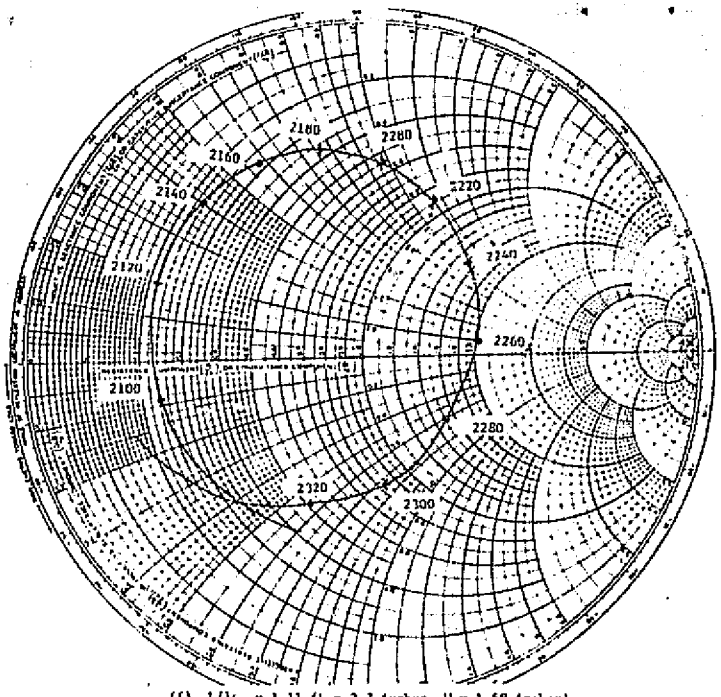

(f) $L/\lambda\varepsilon_r$ = 1.11 (L = 3.7 inches, W = 1.58 inches)

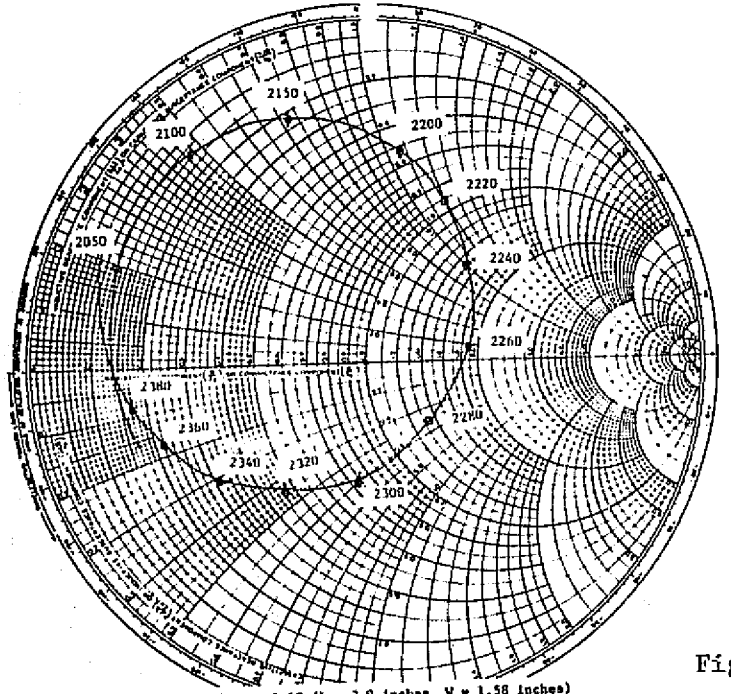

(g) $L/\lambda\varepsilon_r$ = 1.18 (L = 3.9 inches, W = 1.58 inches)

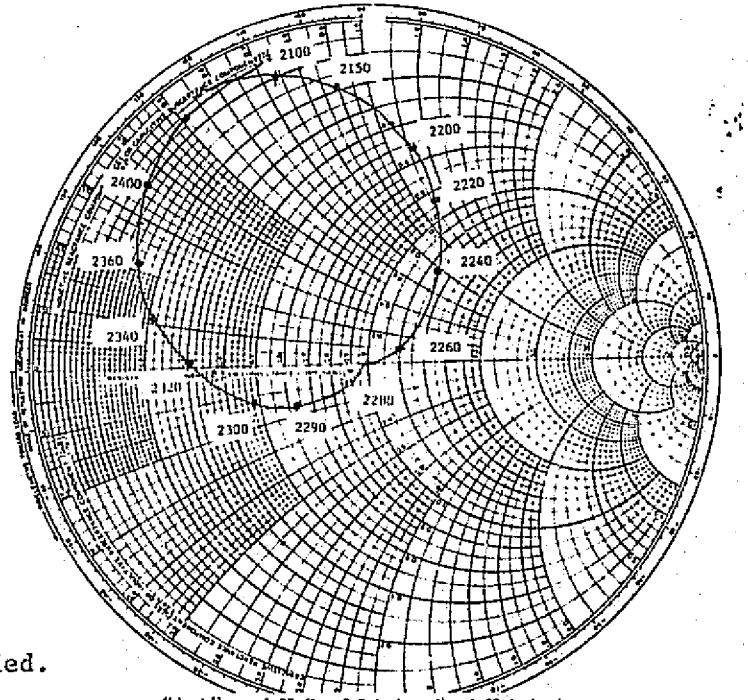

(h) $L/\lambda\varepsilon r$ = 1.52 (L = 5.0 inches, W = 1.58 inches)

Figure 2. - Concluded.

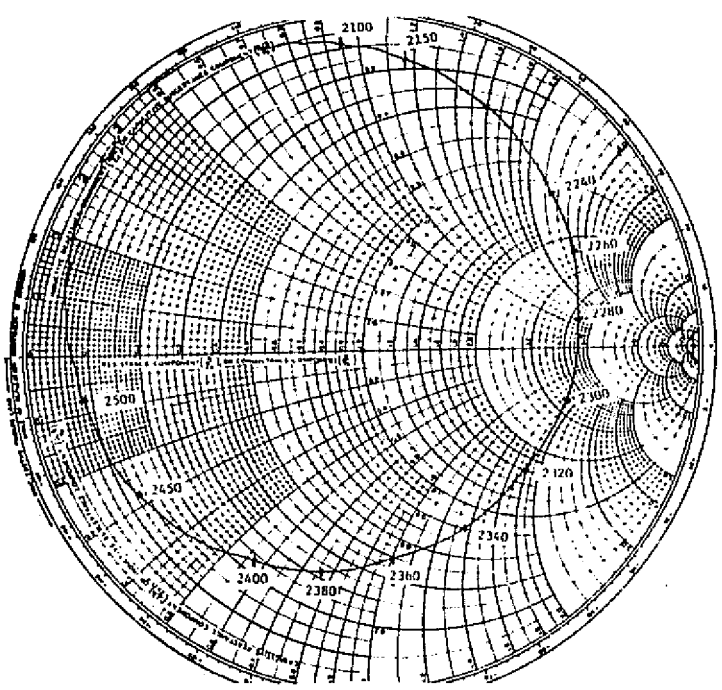

(a) $(L/\lambda_{cr}) = 0.57$ (L = 1.90, W = 1.58)

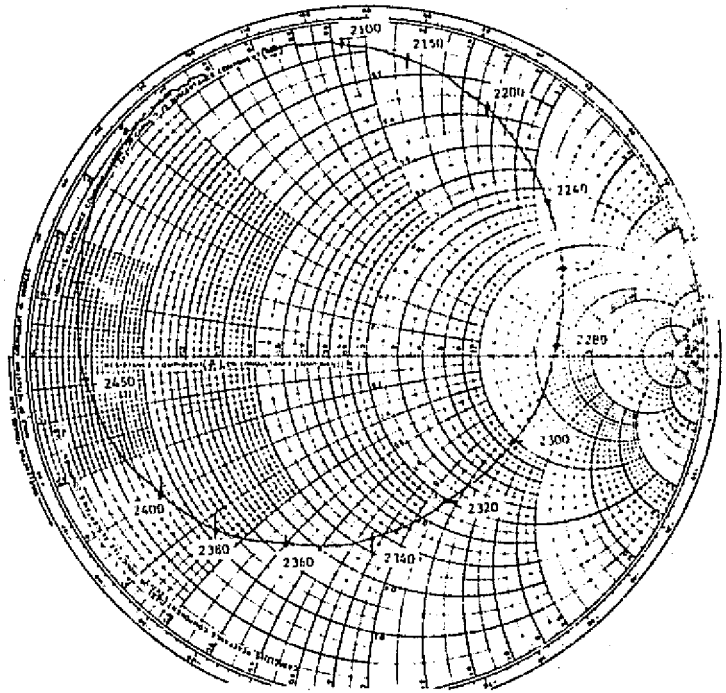

(b) $L/\lambda_{cr} = 0.75$ (L = 2.3, W = 1.58)

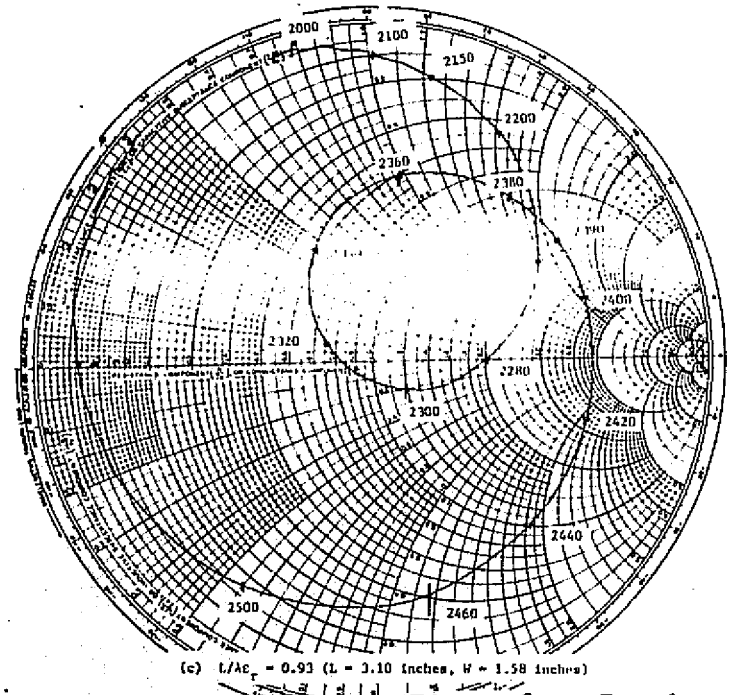

(c) $L/\lambda_{c_r} = 0.93$ (L = 3.10 inches, W = 1.58 inches)

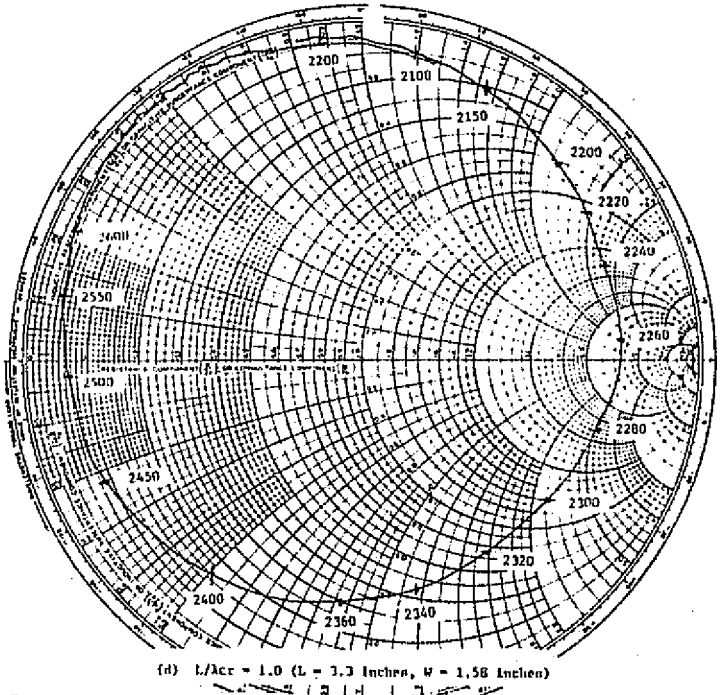

(d) $L/\lambda_{cr} = 1.0$ (L = 3.3 inches, W = 1.58 inches)

Figure 2. - Impedance characteristics for a rectangular microstrip resonator as a function of (L/λ_{cr}).

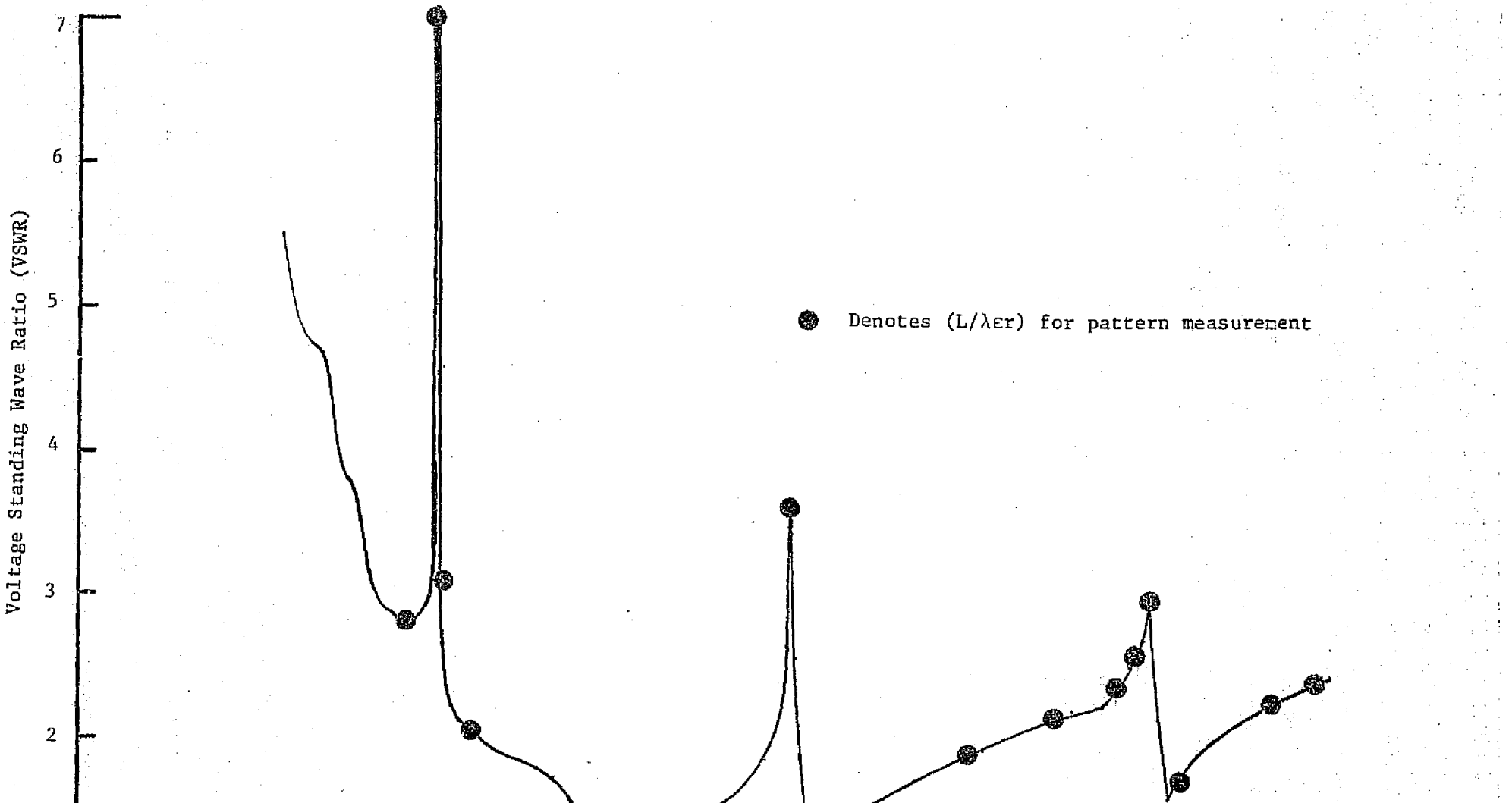

Figure 3. - VSWR versus (L/λεr) for a rectangular microstrip resonator configuration.

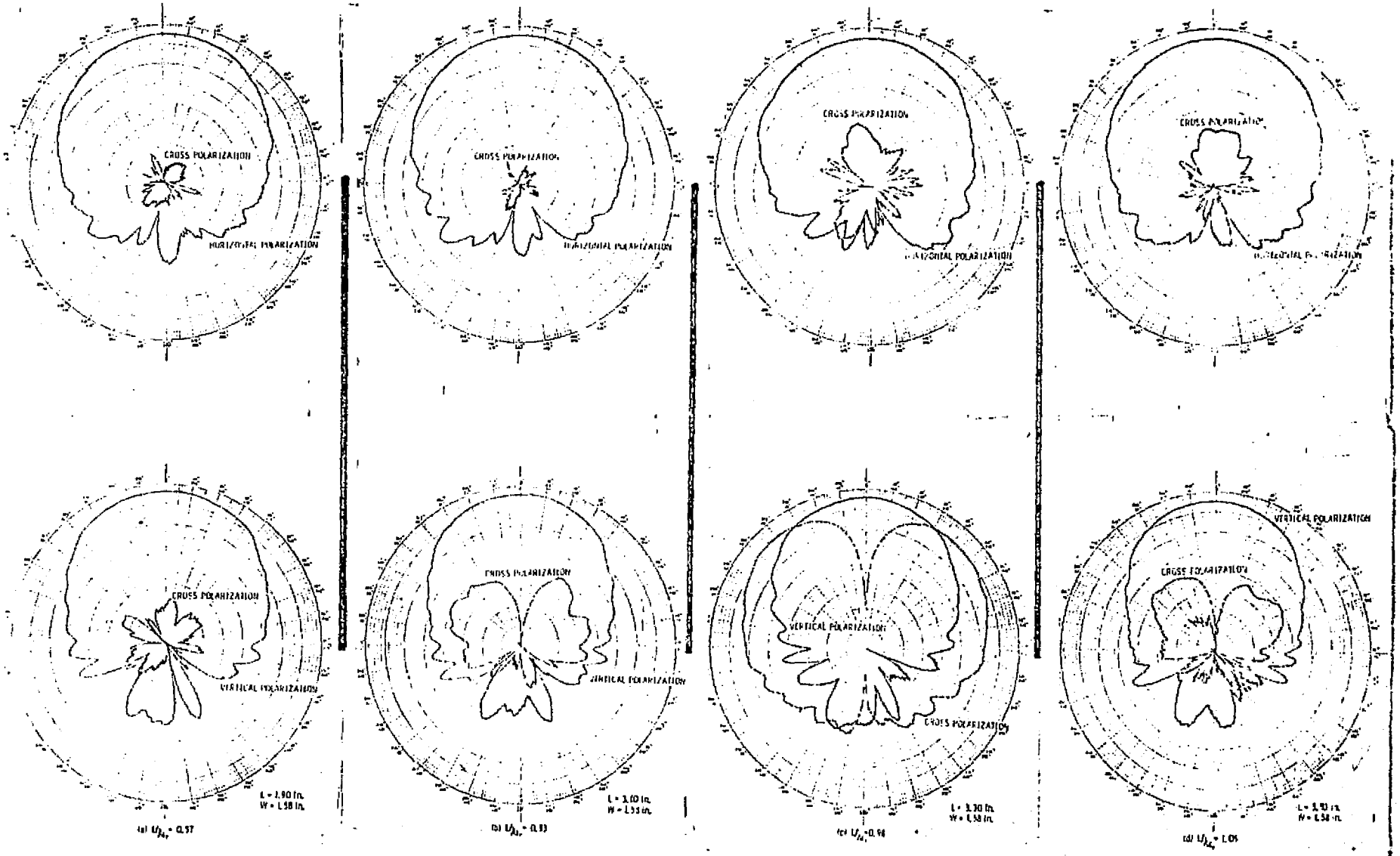

Figure 4. - Radiation pattern characteristics of a rectangular microstrip element for several values of ($L/\lambda\varepsilon_r$).

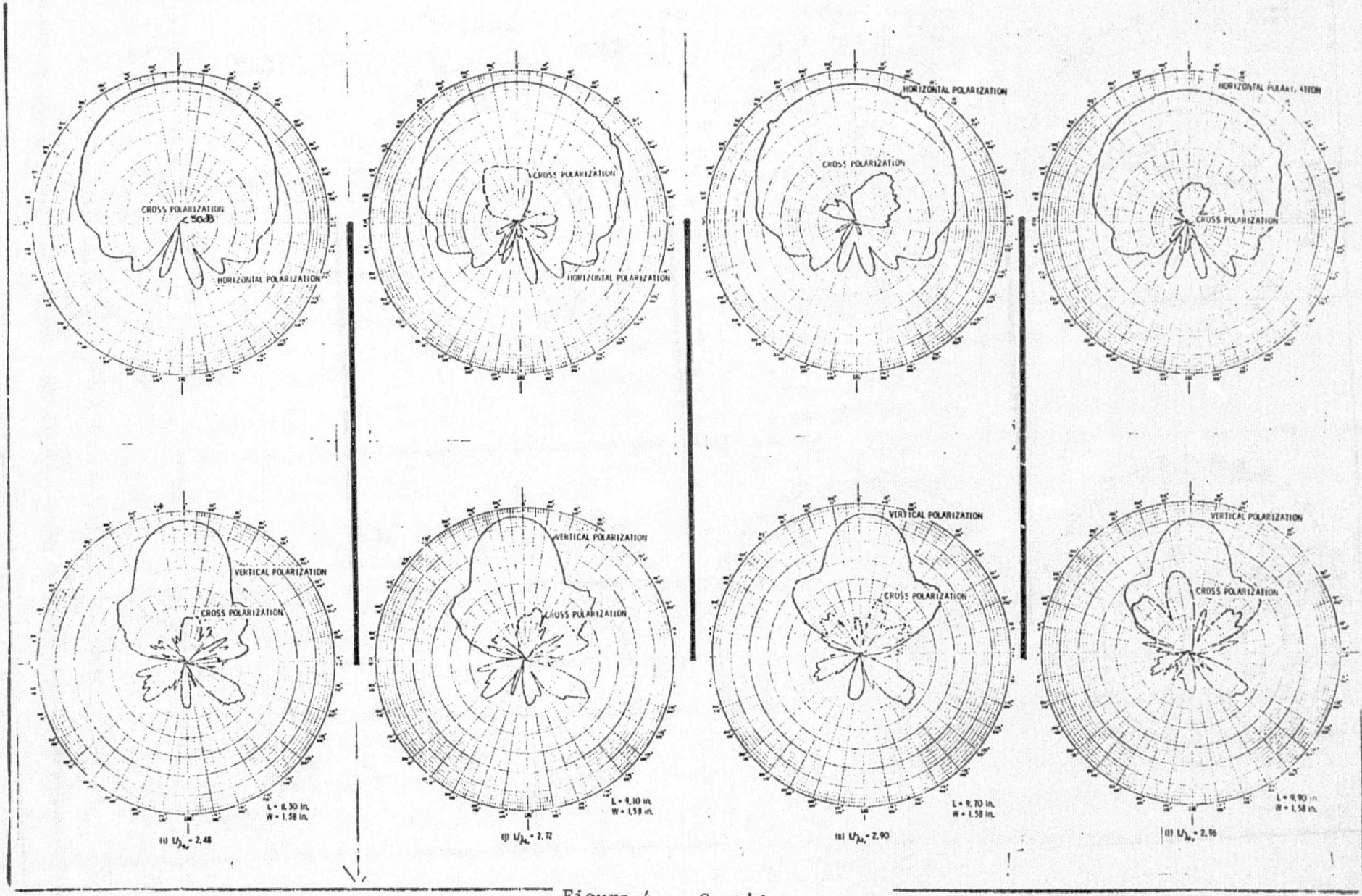

Figure 4. - Cont'd.

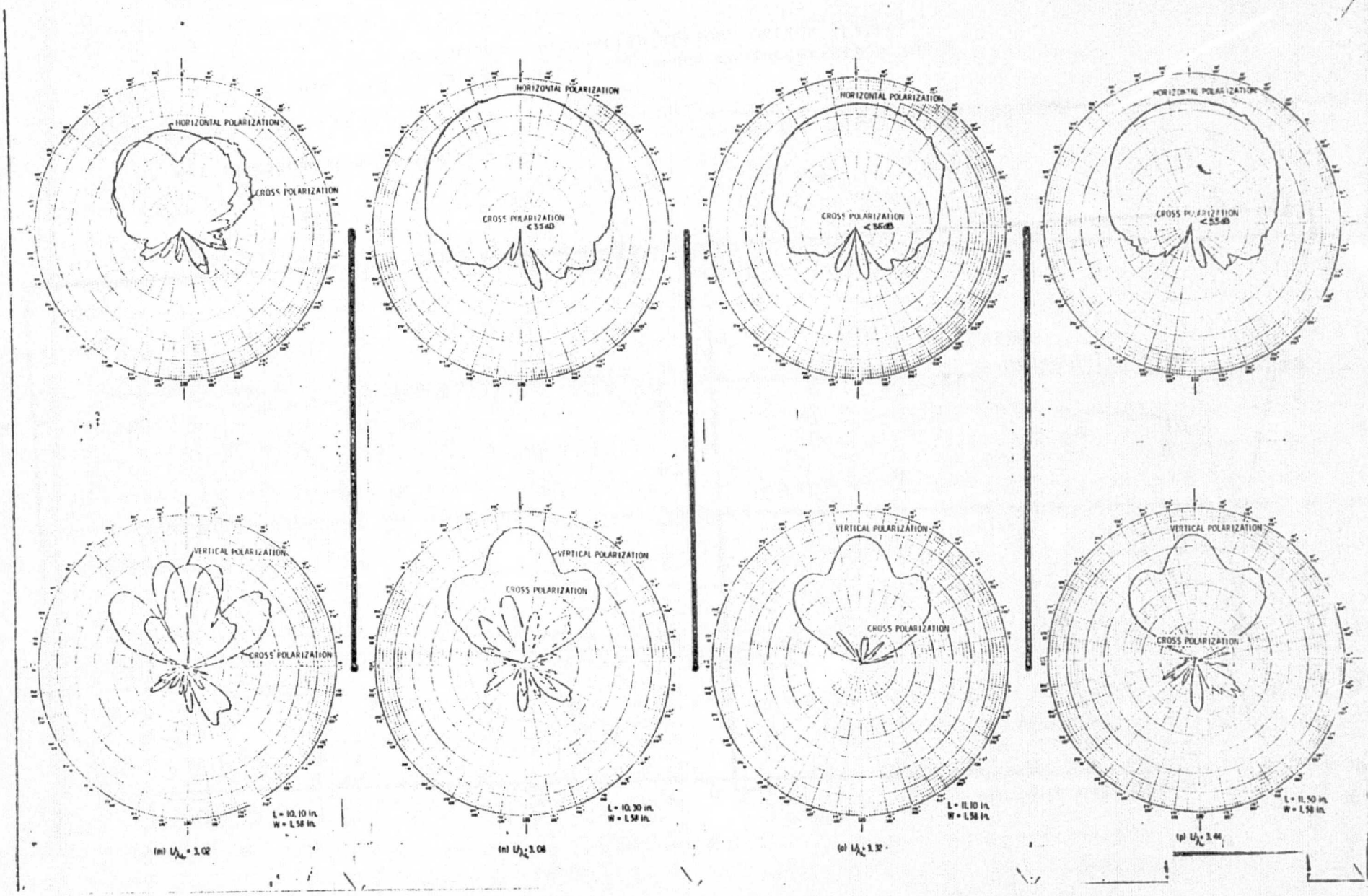

Figure 4. - Concluded

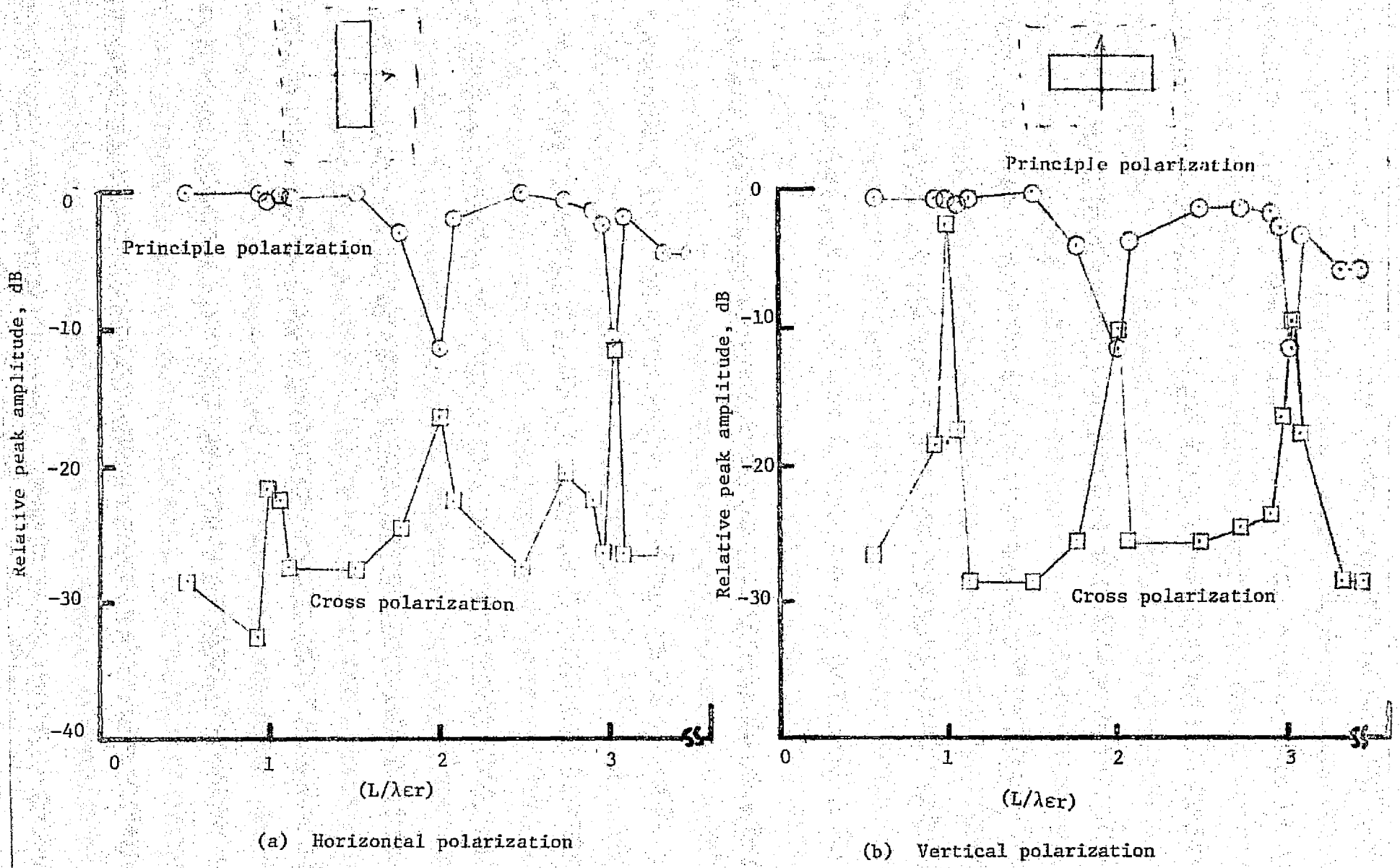

Figure 5. - Radiation pattern amplitude characteristics for a rectangular microstrip element versus (L/λεr).

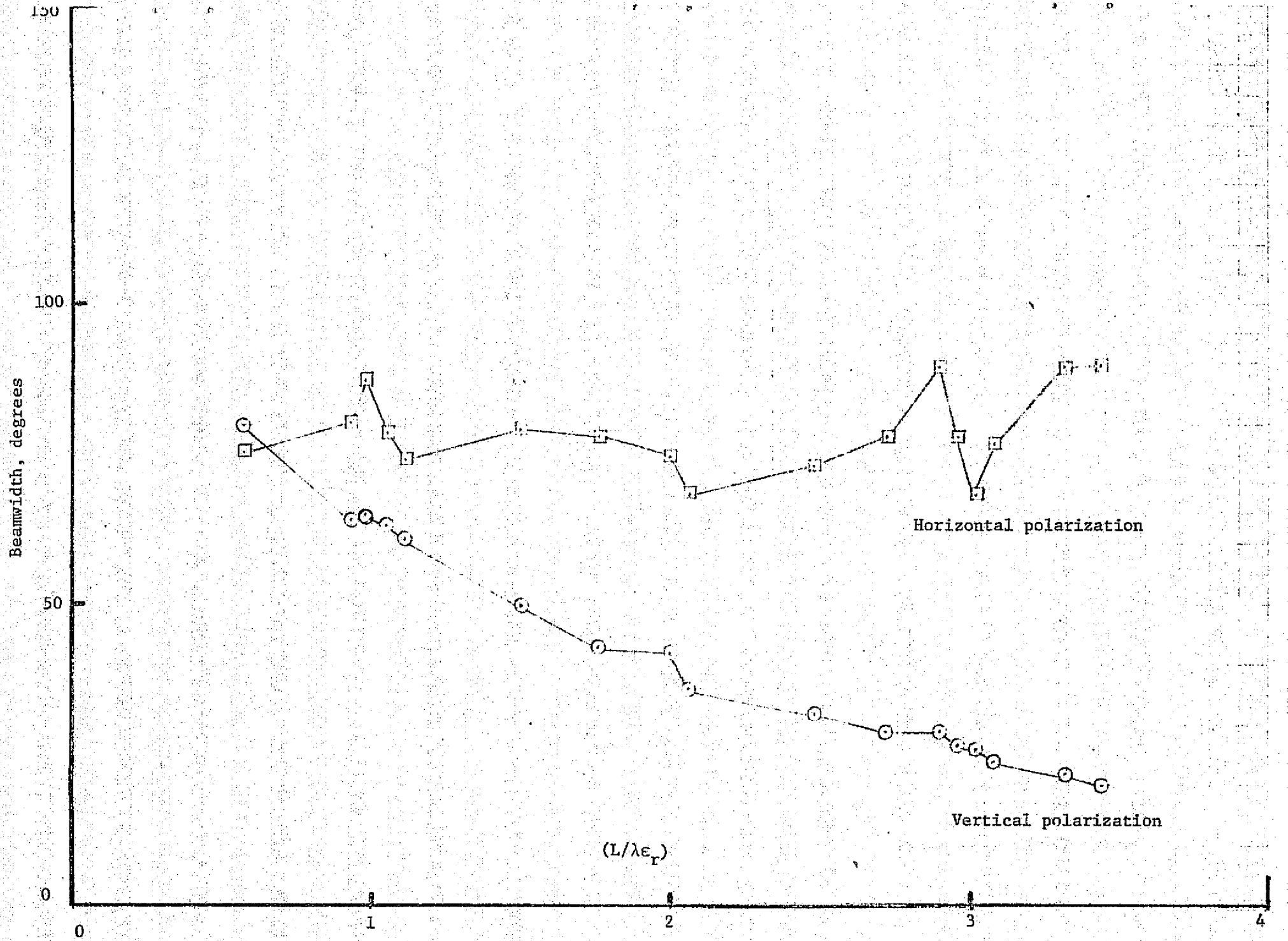

Figure 6. - Beamwidth (HPBW) for a rectangular microstrip element versus $(L/\lambda\varepsilon r)$.

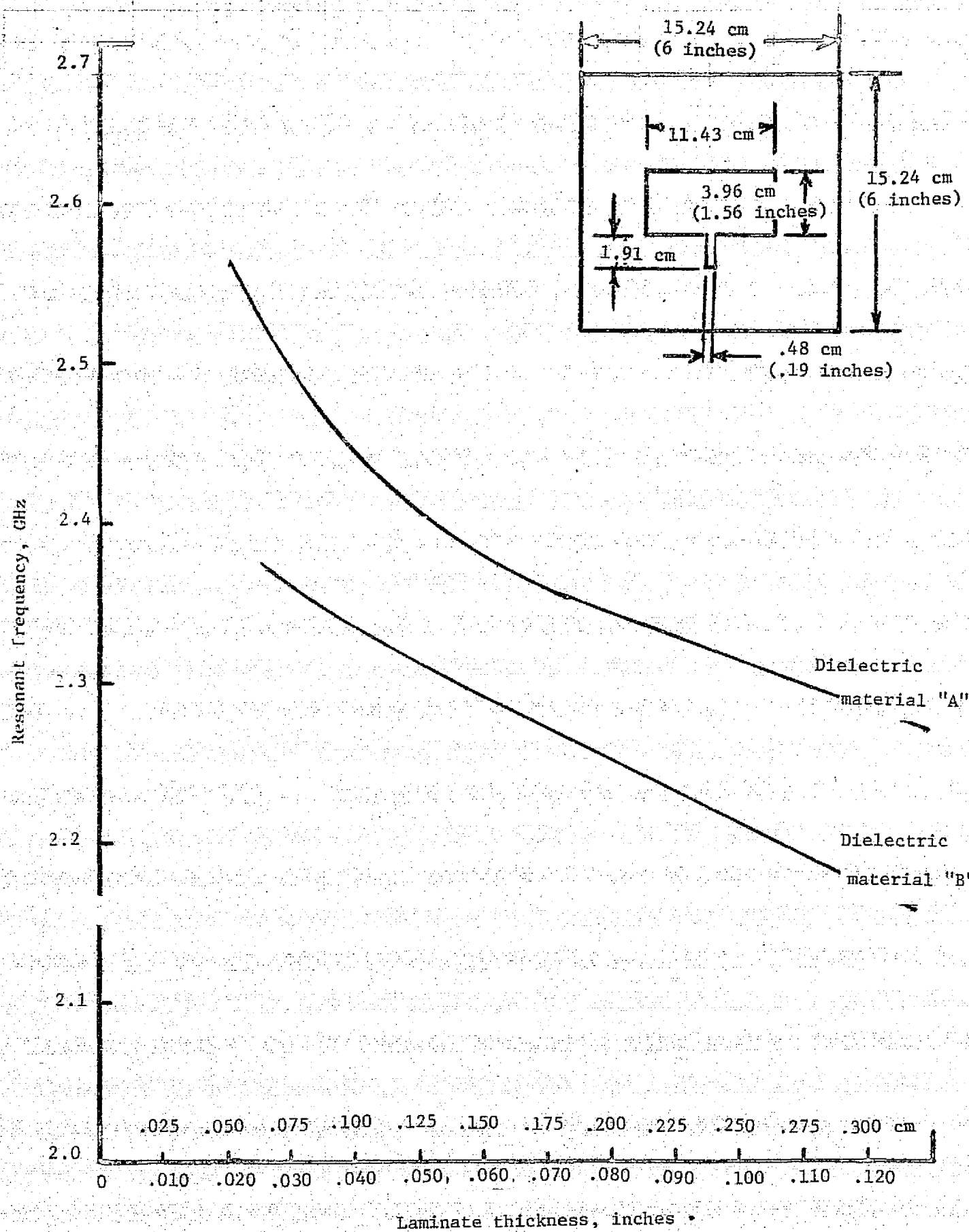

Figure 7. - Resonant frequency for a rectangular microstrip element versus laminate thickness.

Figure 8. - Photograph of thermal qualification test configuration.

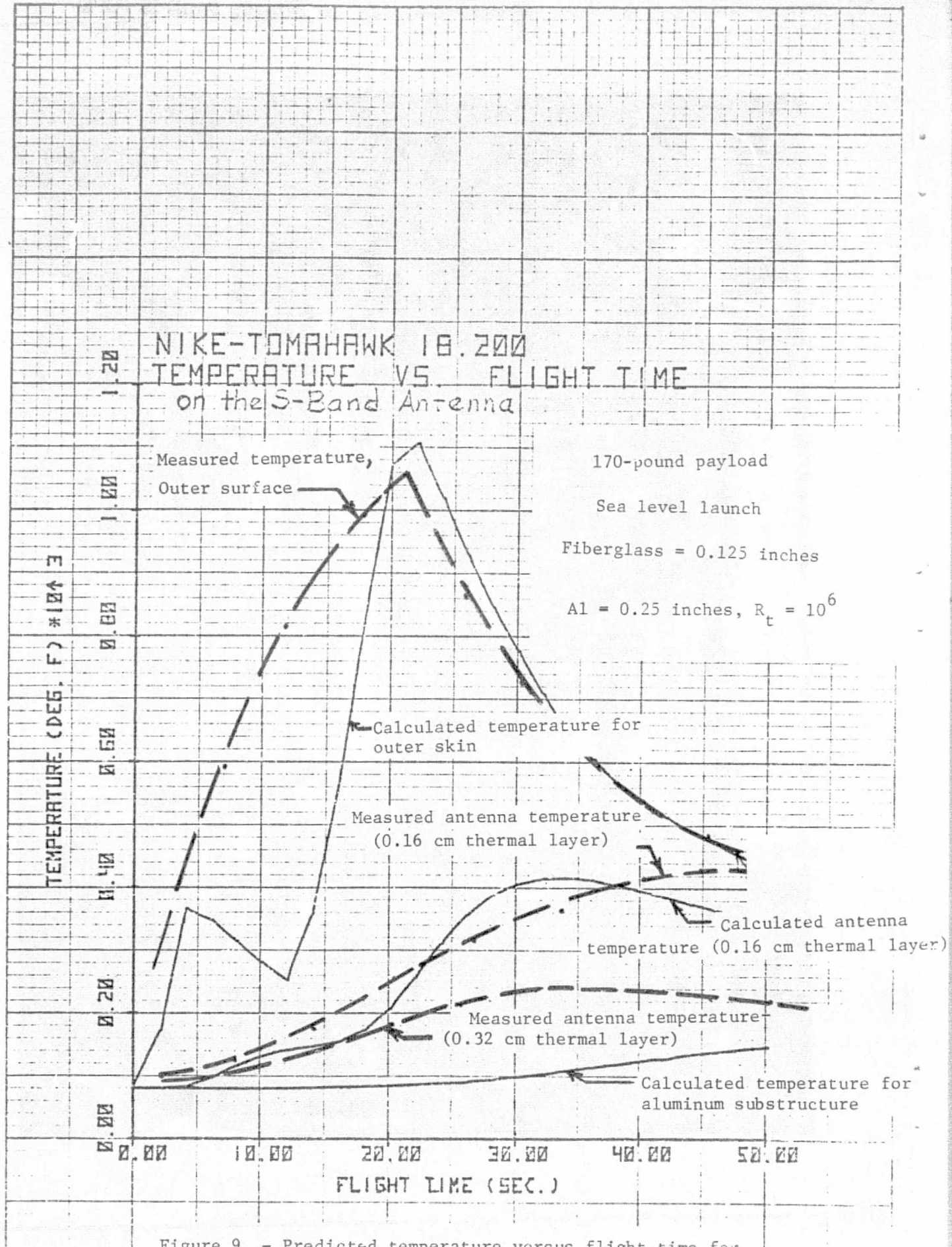

Figure 9. - Predicted temperature versus flight time for Nike-Hawk missile along with antenna thermal test results.

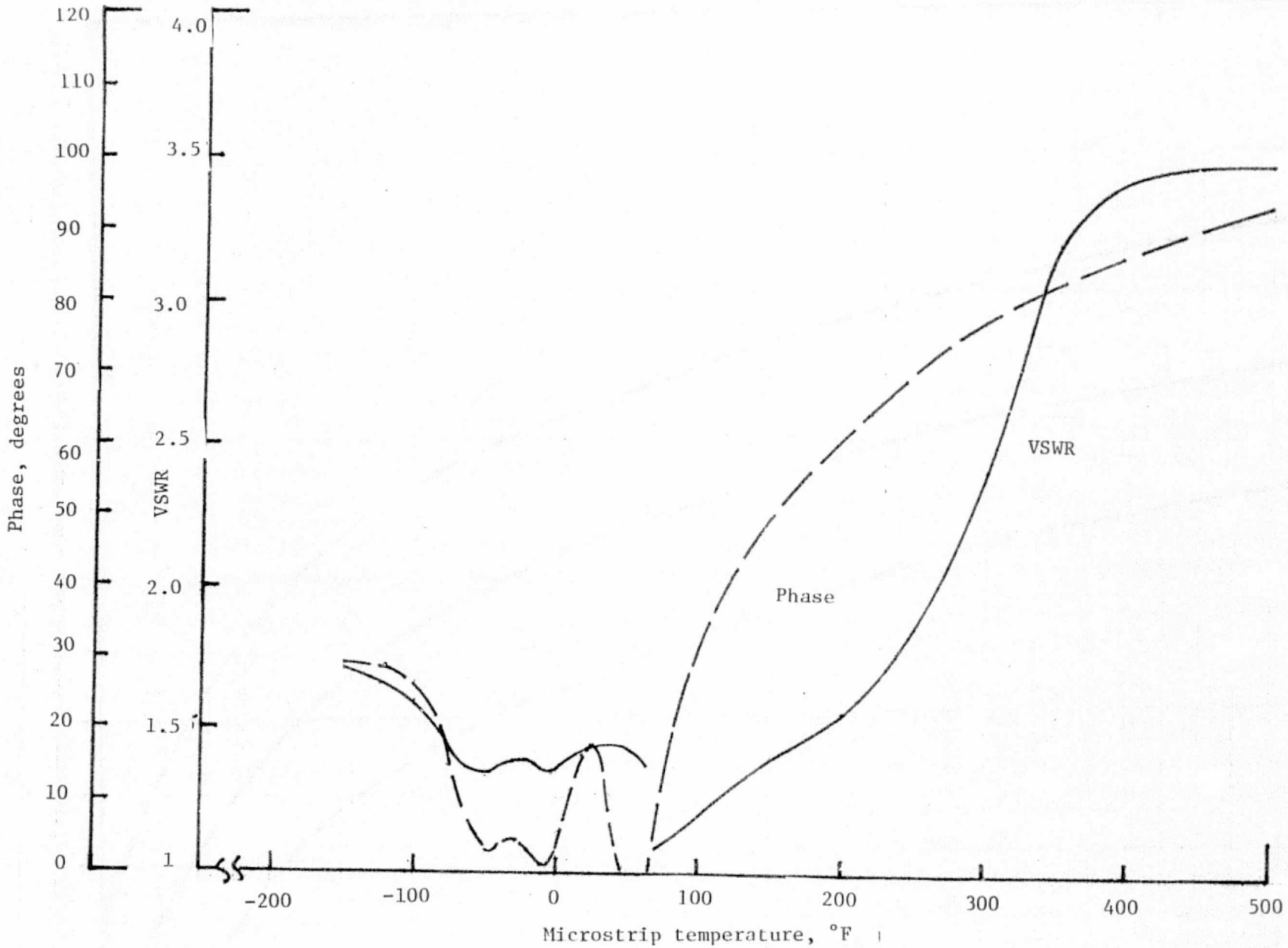

Figure 10. - VSWR and phase versus temperature for a rectangular microstrip antenna element.

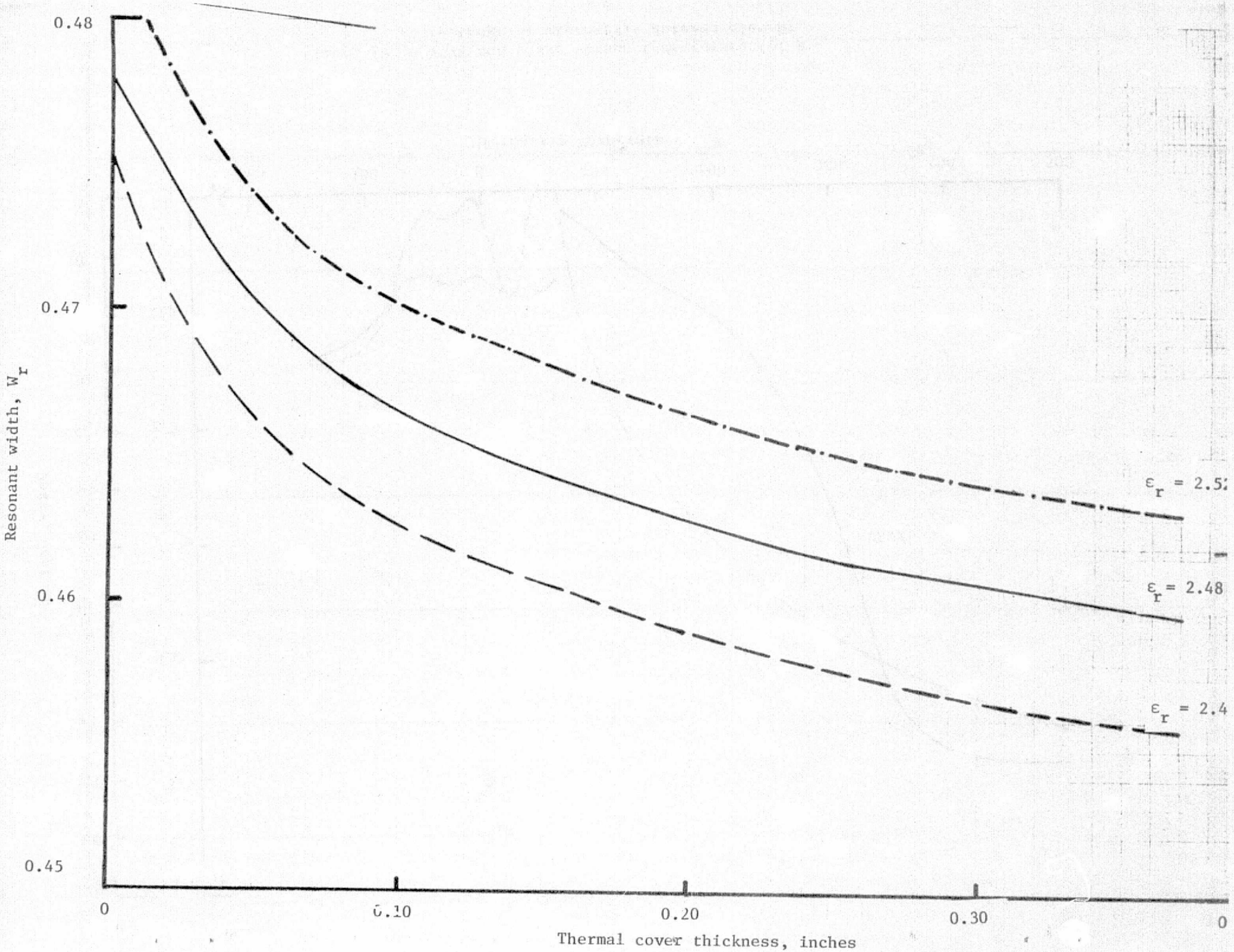
0.48
0.47
0.46
0.45
Resonant width, W_r
ε_r = 2.5
ε_r = 2.48
ε_r = 2.4
0
0.10
0.20
0.30
0
Thermal cover thickness, inches

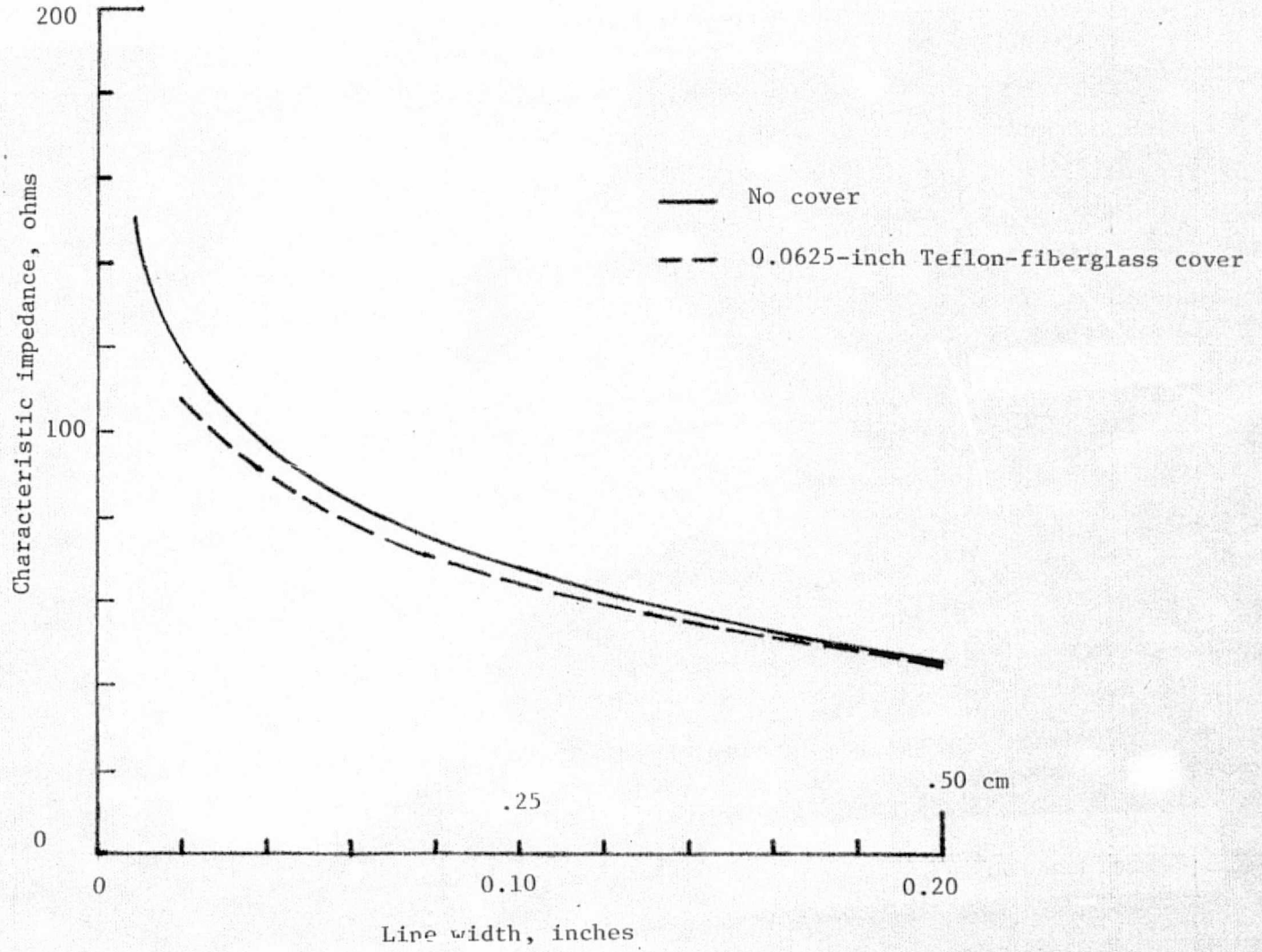

Figure 12. - Characteristic impedance of microstrip lines with and without the thermal cover.

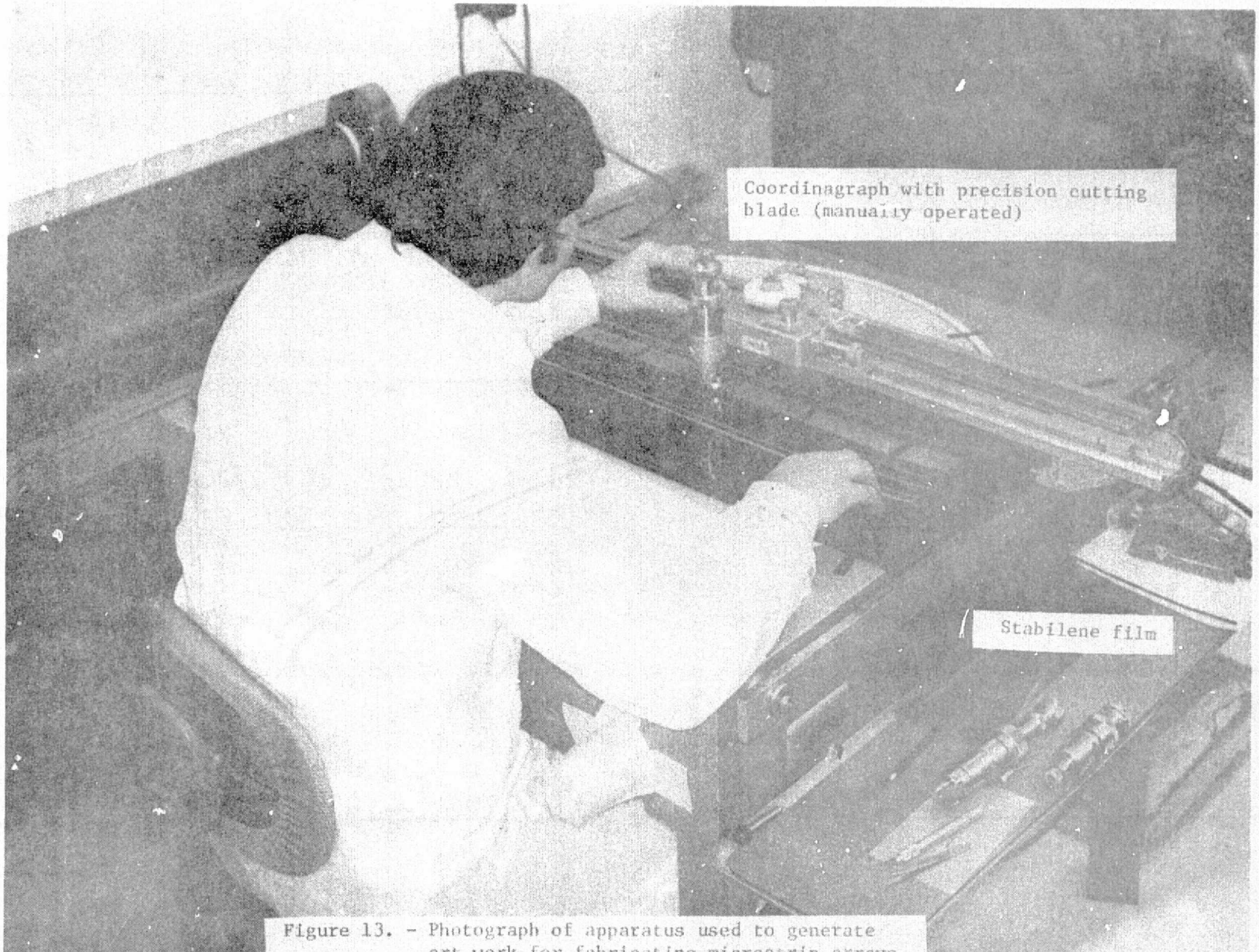

Figure 13. - Photograph of apparatus used to generate art work for fabricating microstrip arrays.

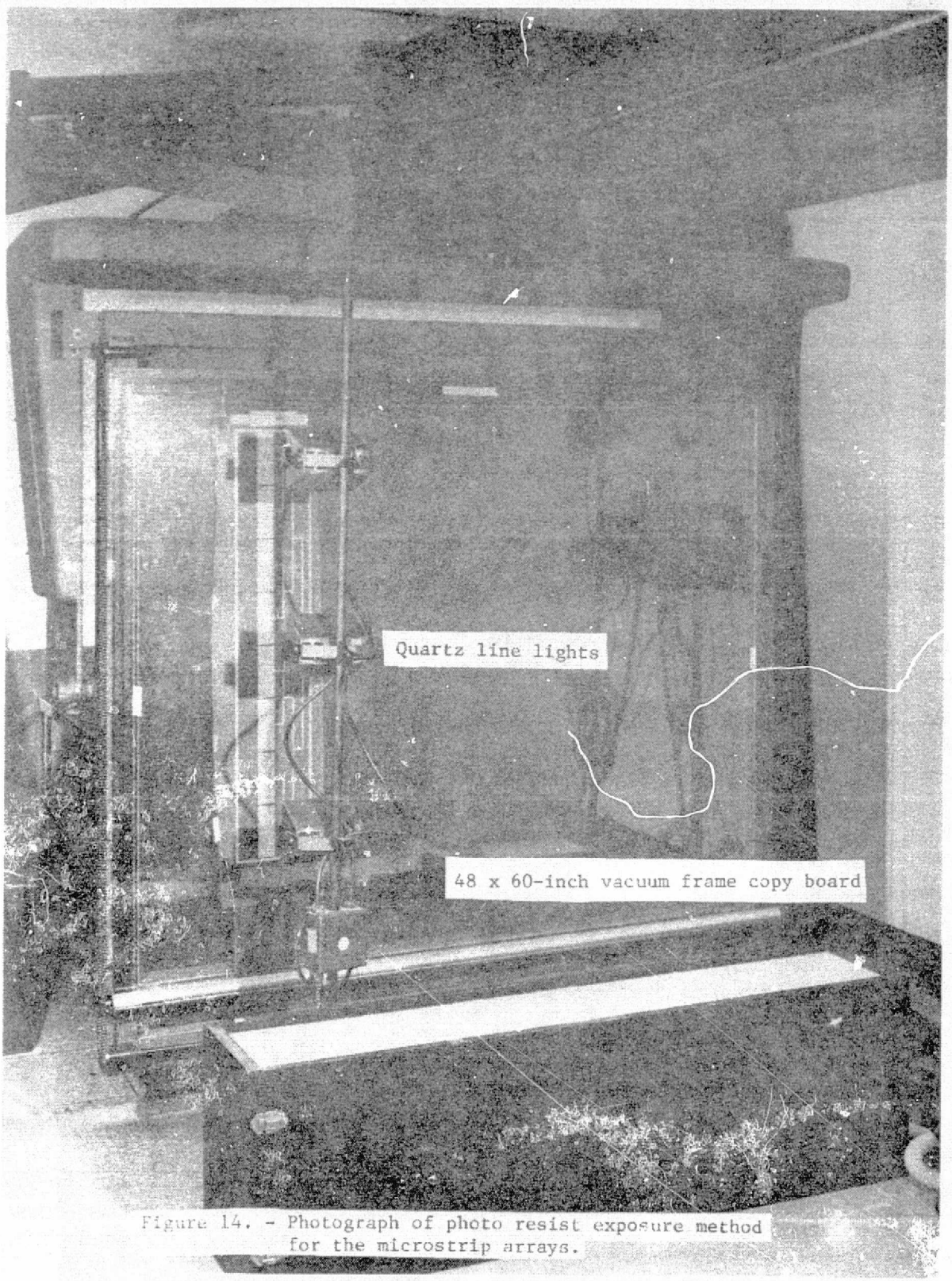

Figure 14. - Photograph of photo resist exposure method for the microstrip arrays.

Figure 15. - Photograph of photo resist application process.

Figure 16. - Photograph of the chemical etching process.

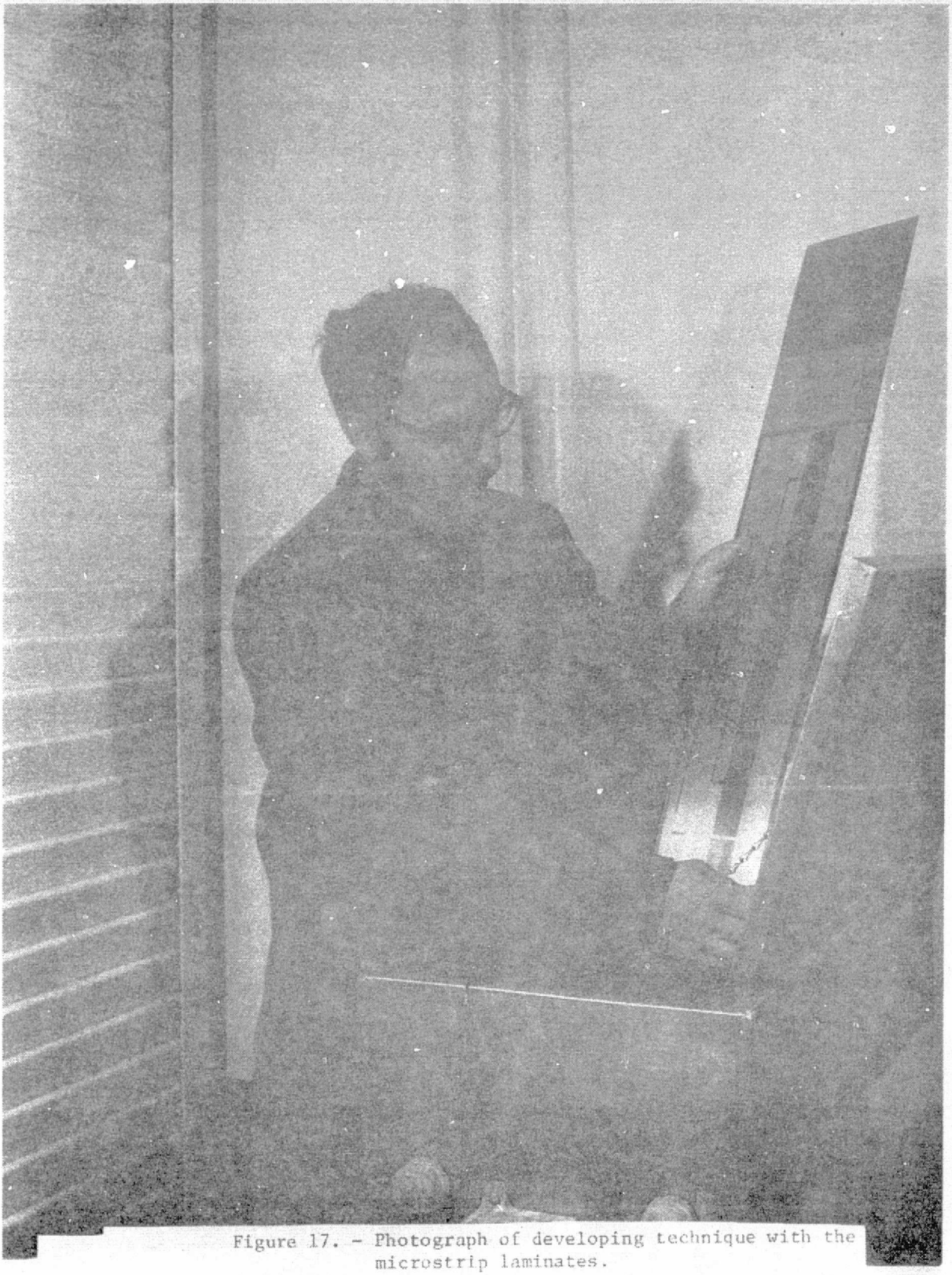

Figure 17. - Photograph of developing technique with the microstrip laminates.

Figure 18. - Photograph of the antenna dimensional check using the Cordax System.

Figure 19. - Photograph of the antenna gold-plating process.

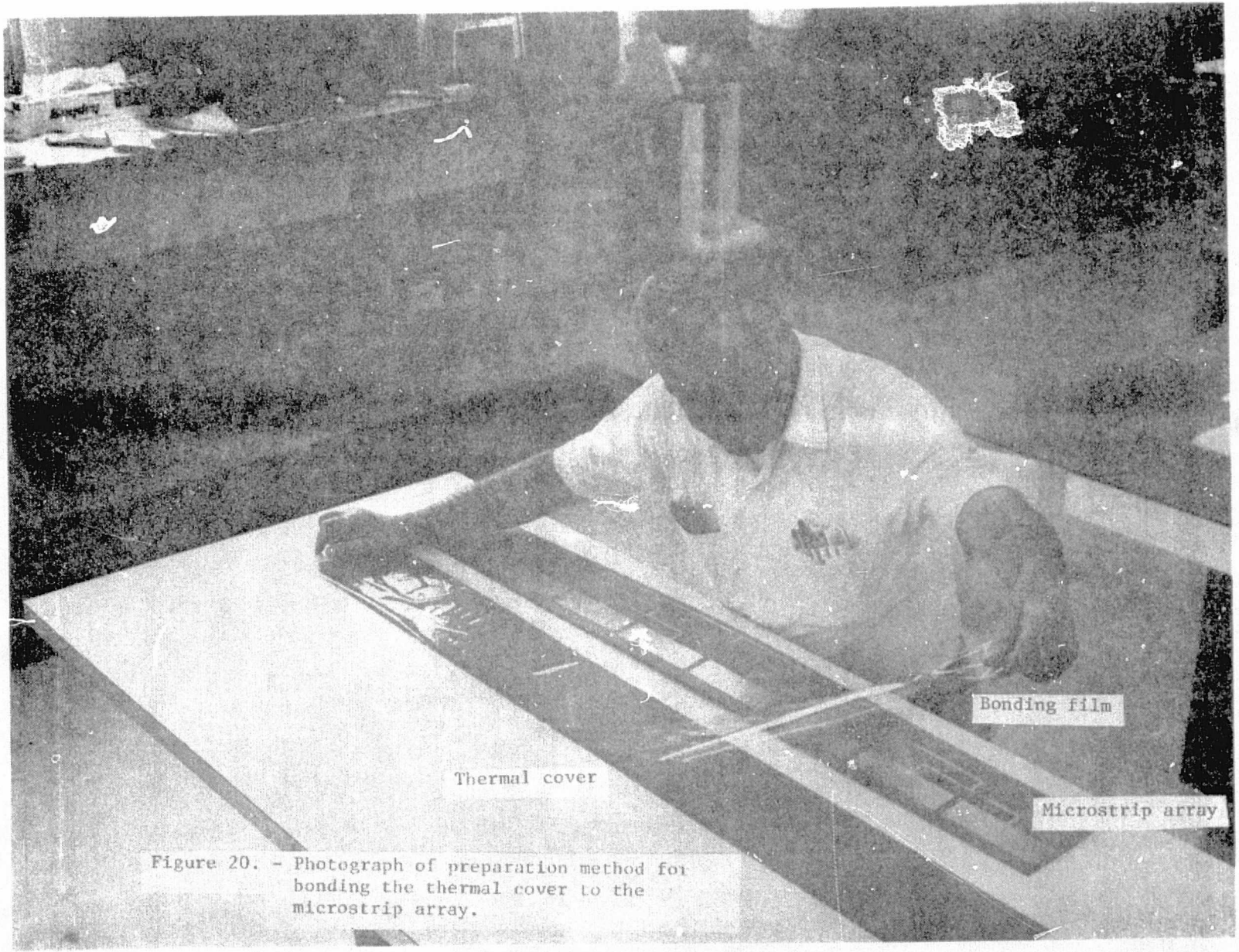

Figure 20. - Photograph of preparation method for bonding the thermal cover to the microstrip array.

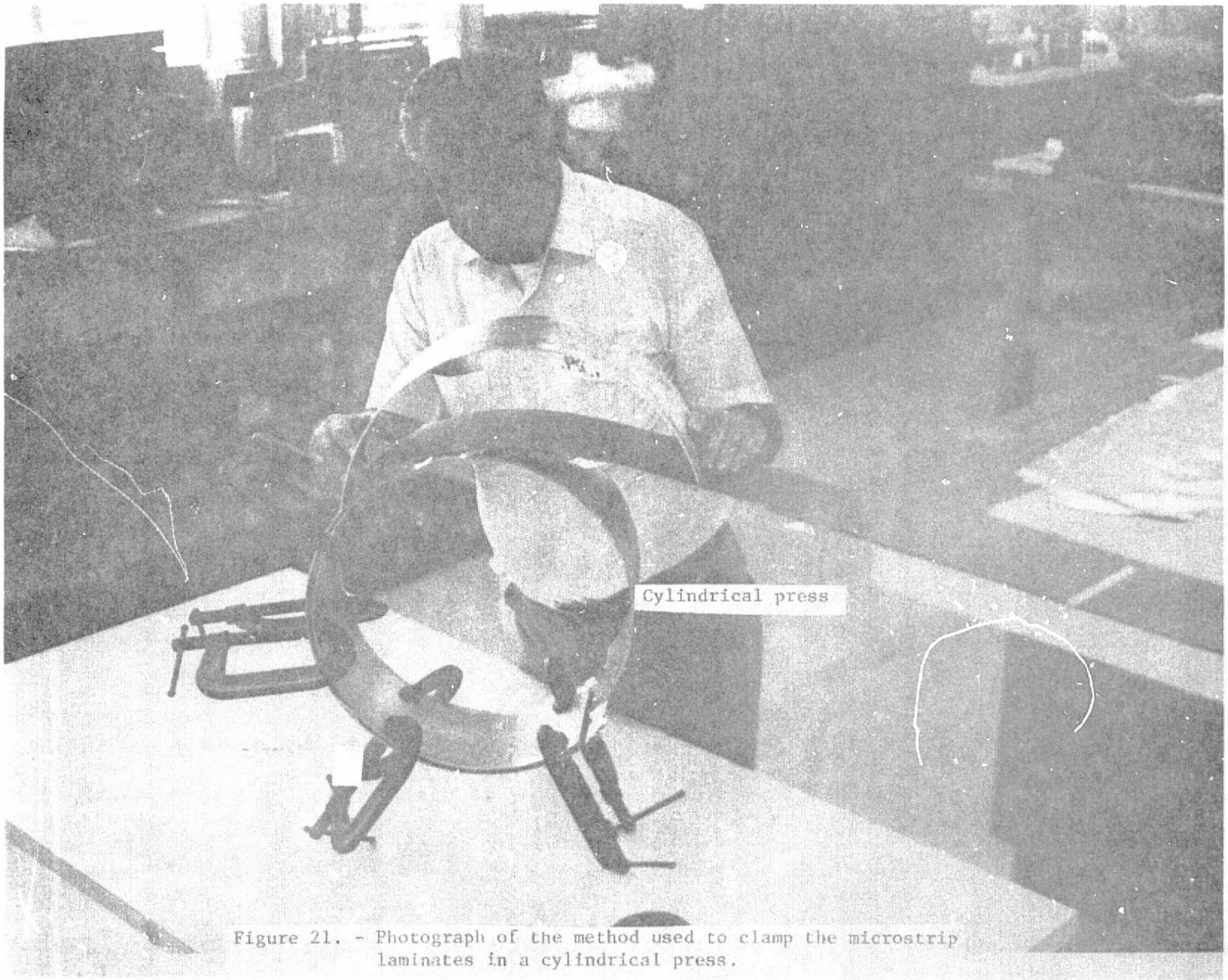

Figure 21. - Photograph of the method used to clamp the microstrip laminates in a cylindrical press.

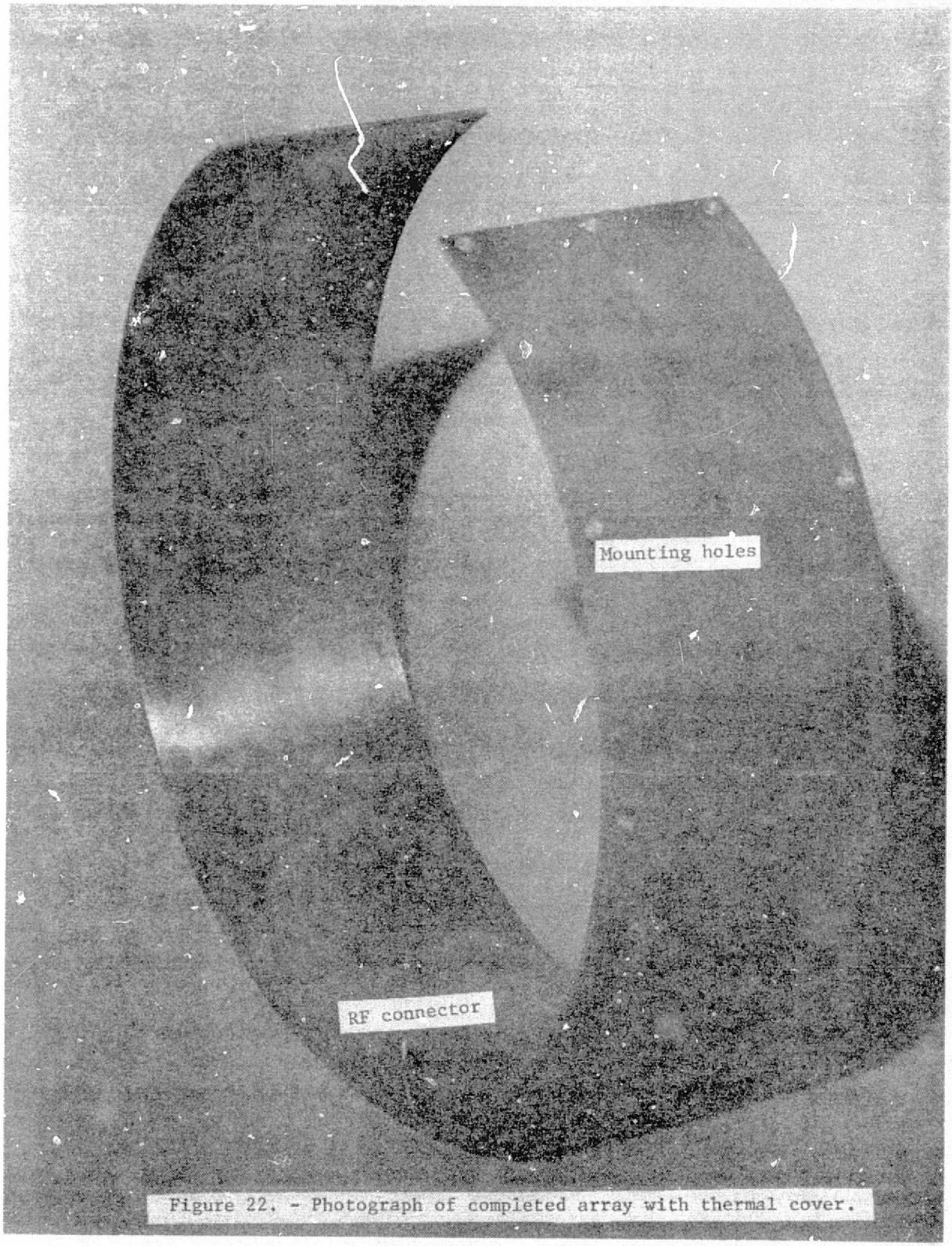

Figure 22. - Photograph of completed array with thermal cover.

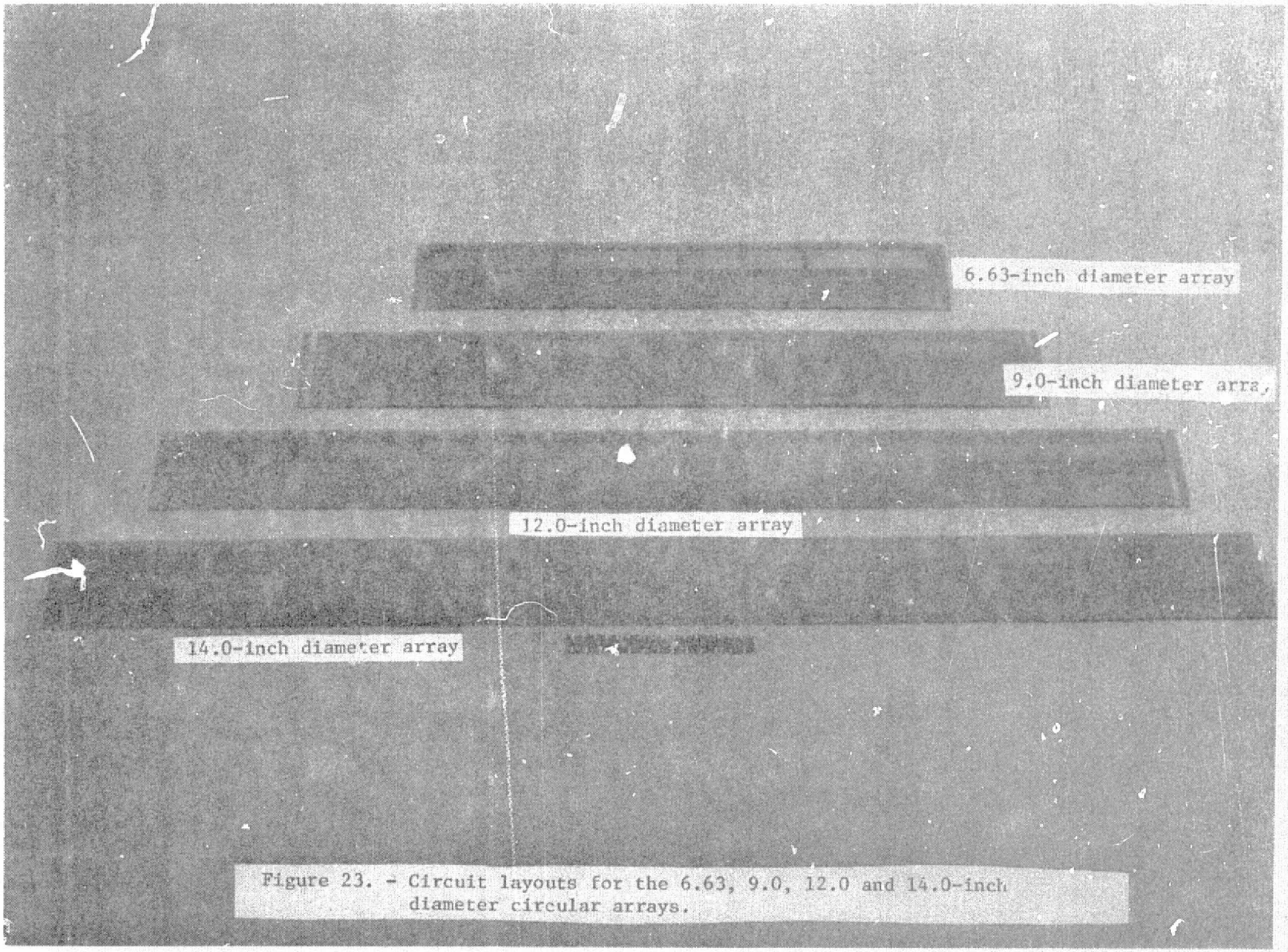

Figure 23. - Circuit layouts for the 6.63, 9.0, 12.0 and 14.0-inch diameter circular arrays.

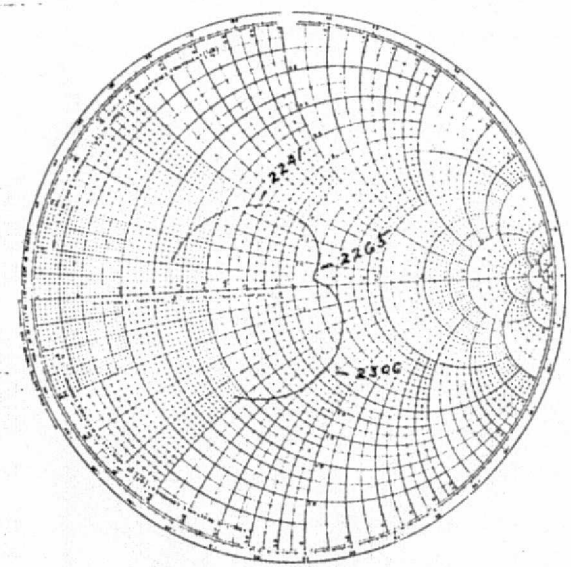

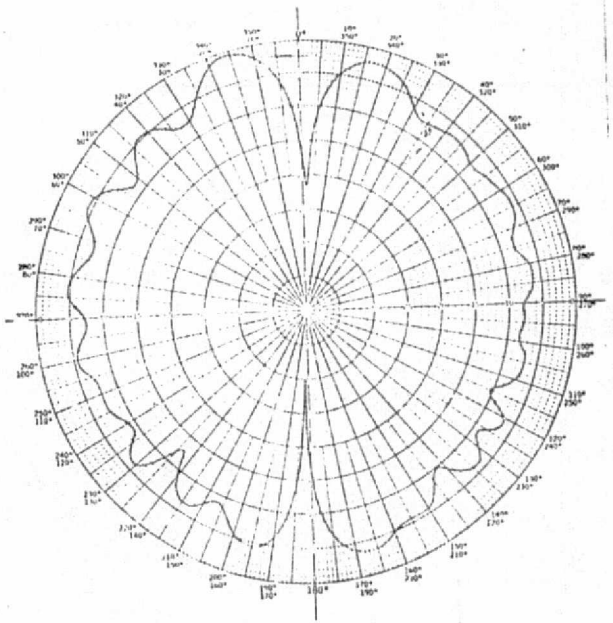

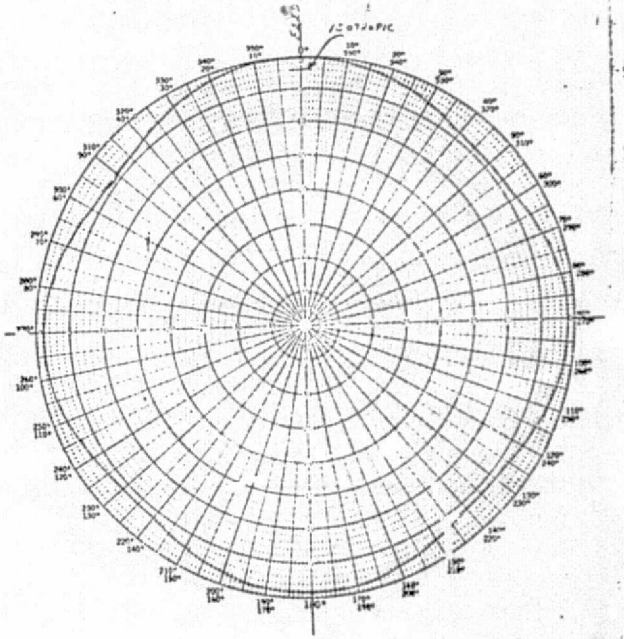

(a) 6.63-inch diameter array

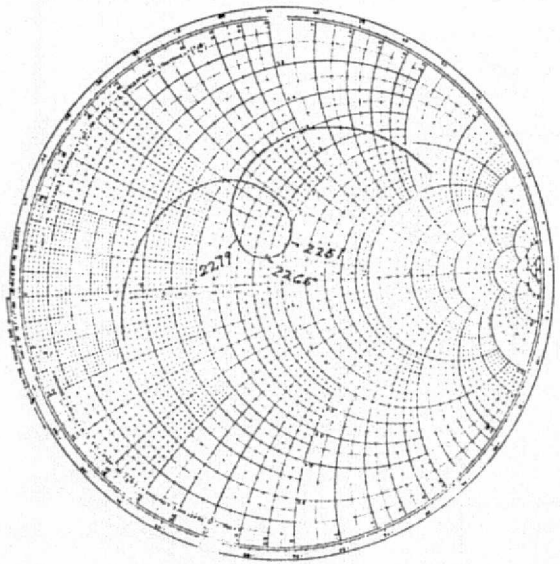

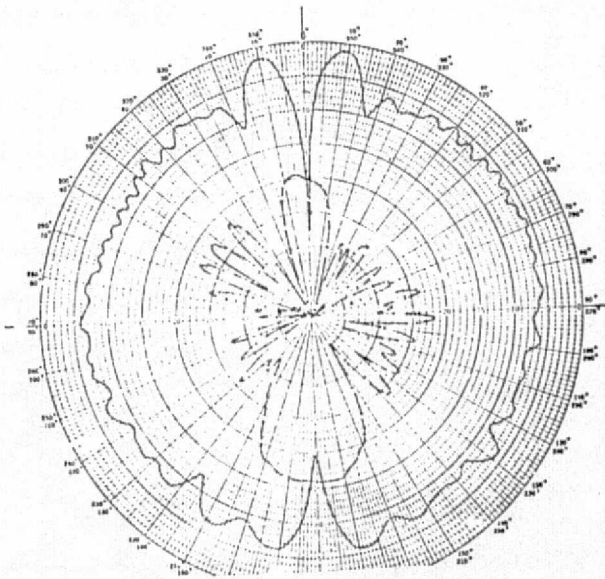

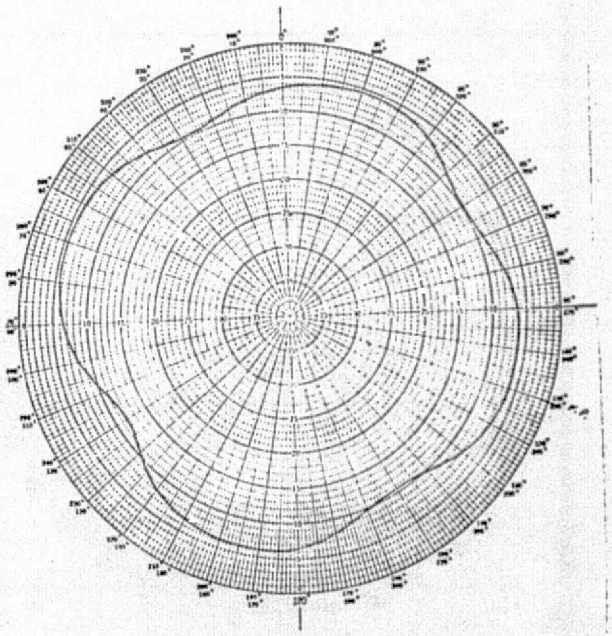

(b) 9.0-inch diameter array

Figure 24. - Typical impedance and radiation pattern characteristics for the 6.63, 9.0, 12.0, and 14.0-inch diameter circular arrays.

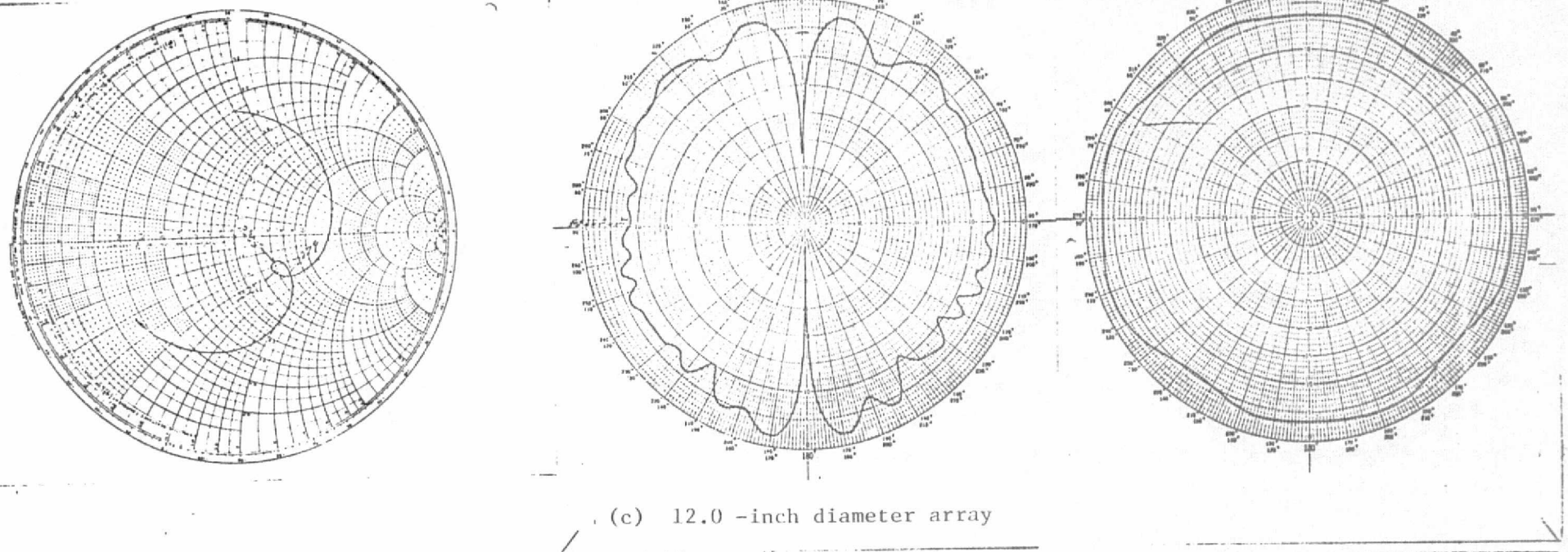

(c) 12.0 -inch diameter array

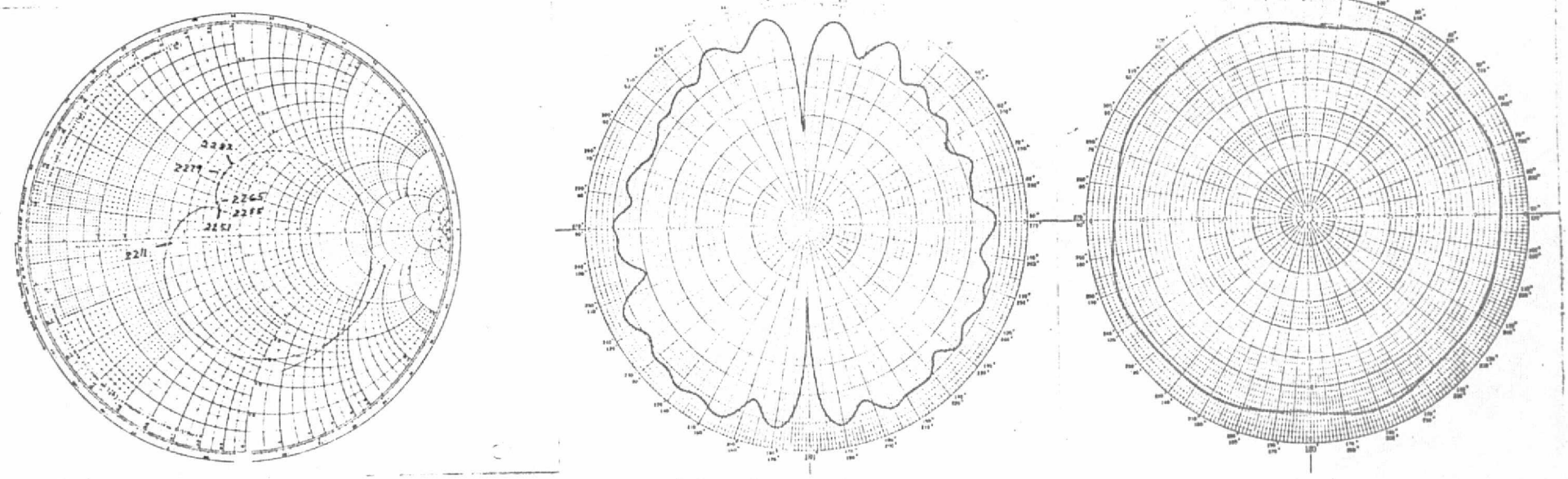

(d) 14-inch diameter array.

Figure 24. - Concluded.

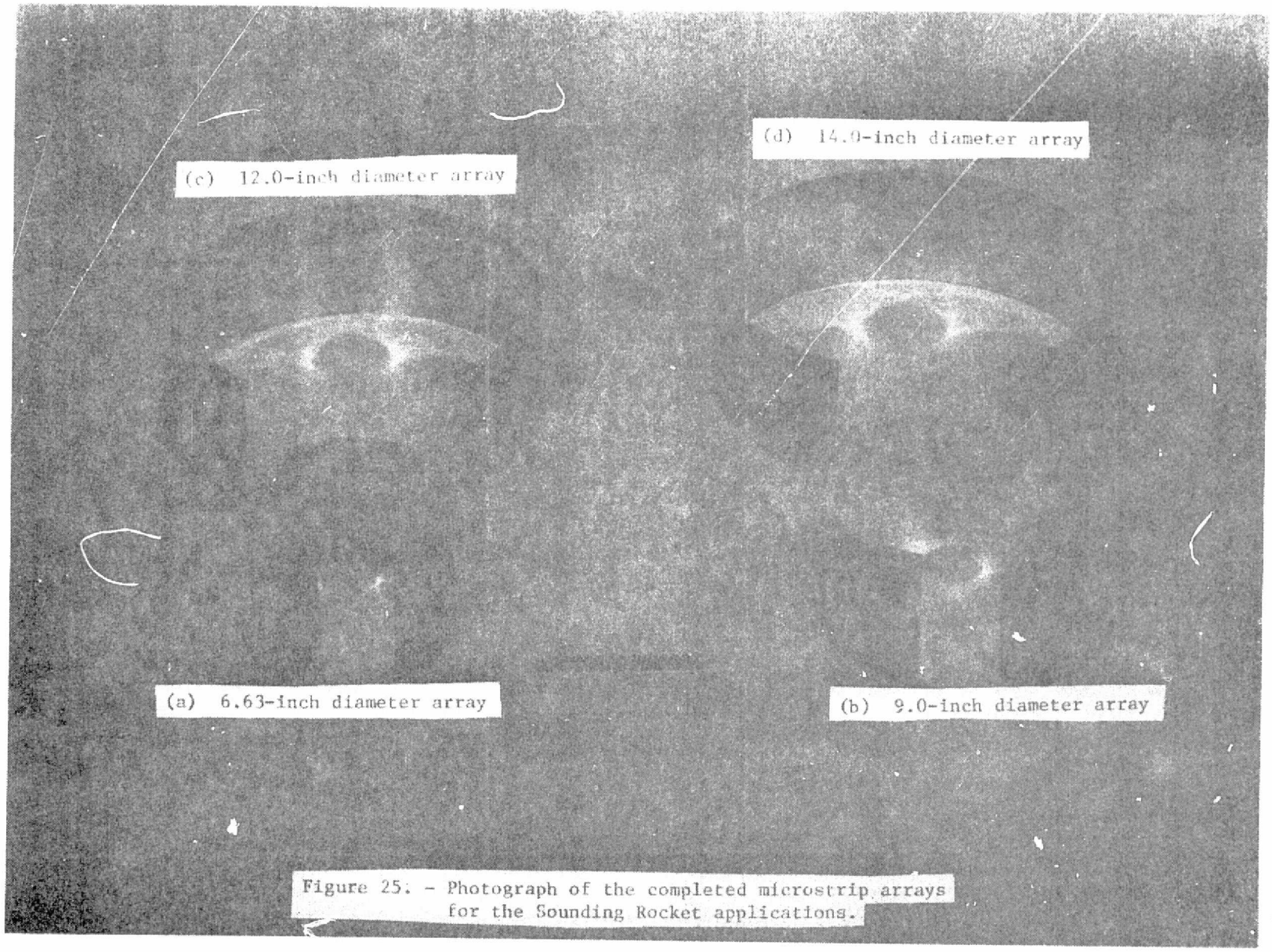

Figure 25. - Photograph of the completed microstrip arrays for the Sounding Rocket applications.

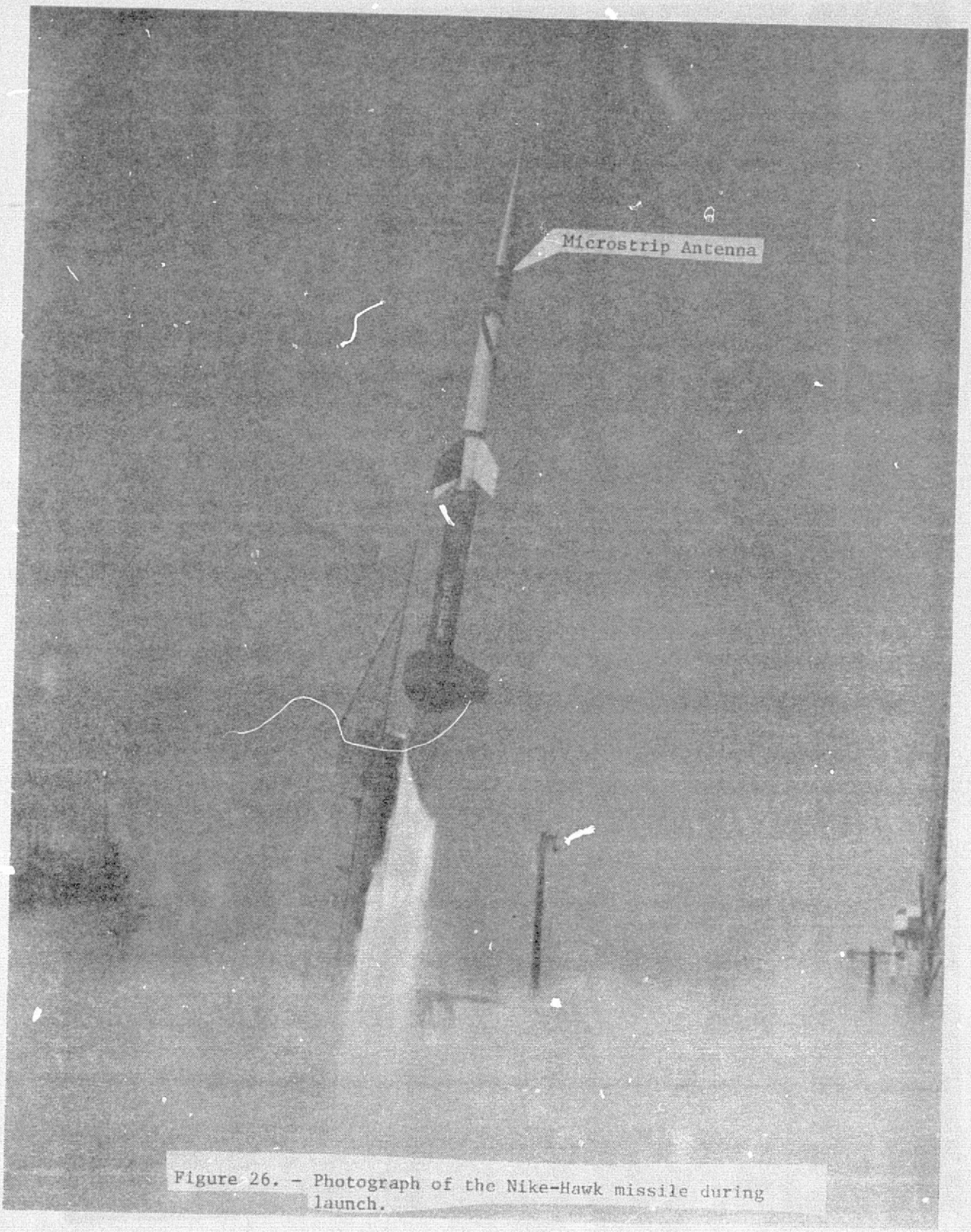

Figure 26. - Photograph of the Nike-Hawk missile during launch.

Figure 27. - Photograph of the S-band microstrip array on the Dual Air Density Satellite 24-element microstrip array (37-inch diameter).

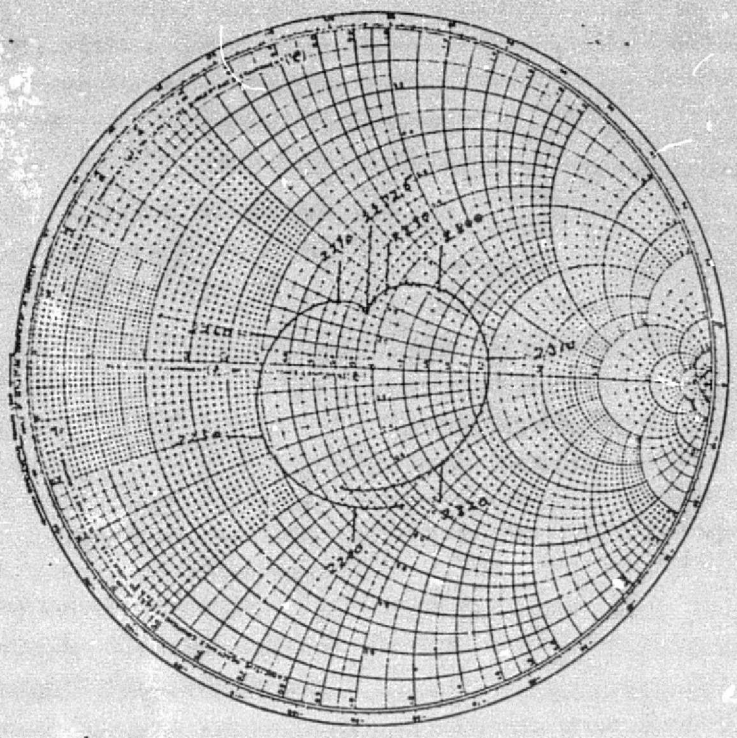

(a) Impedance characteristics of the 24-element microstrip array.

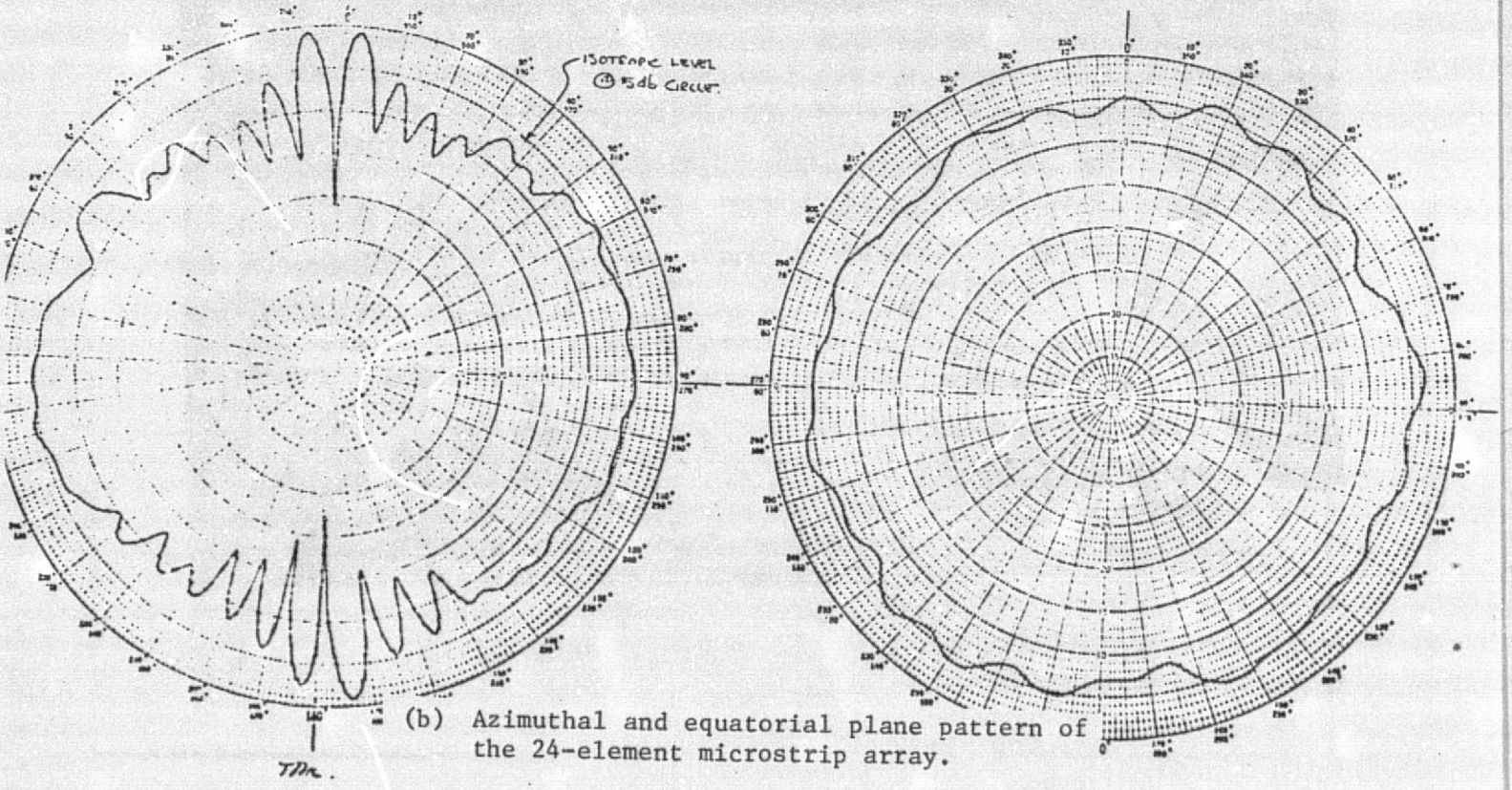

(b) Azimuthal and equatorial plane pattern of the 24-element microstrip array.

Figure 28. - Radiation pattern and impedance characteristics of the 24-element microstrip array of the Dual Air Density Satellite.

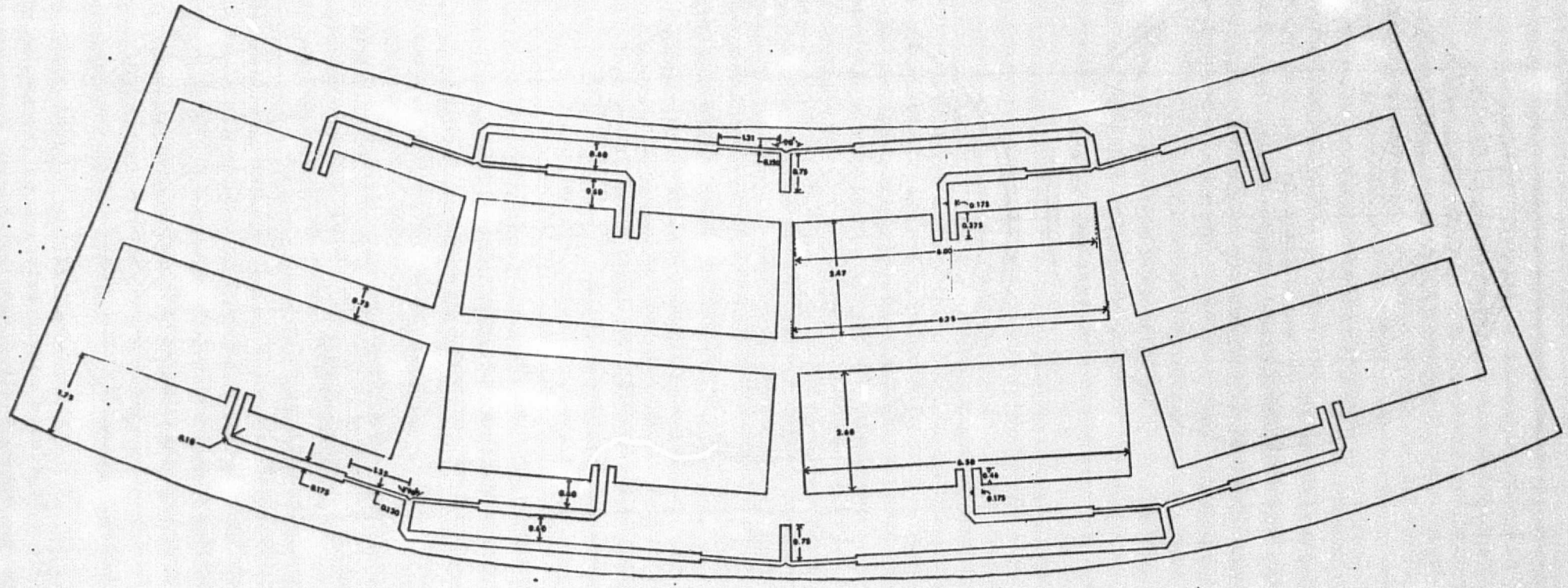

Figure 29. - Circular array configuration for the L-band microstrip antenna for the Aircraft Drone.

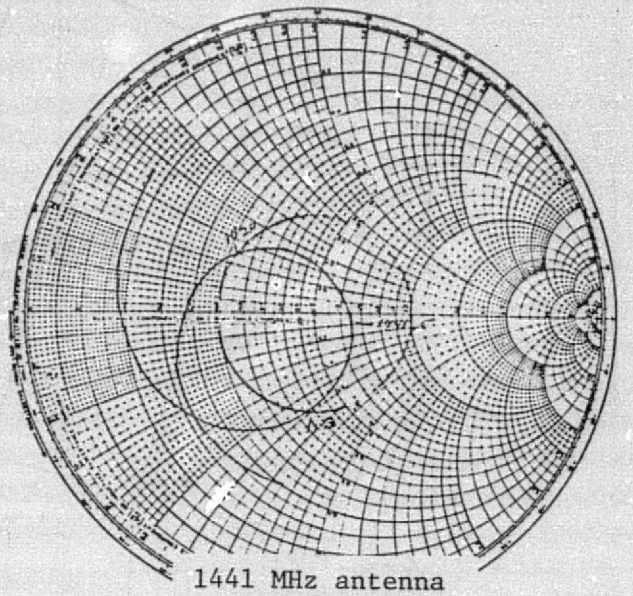

1441 MHz antenna

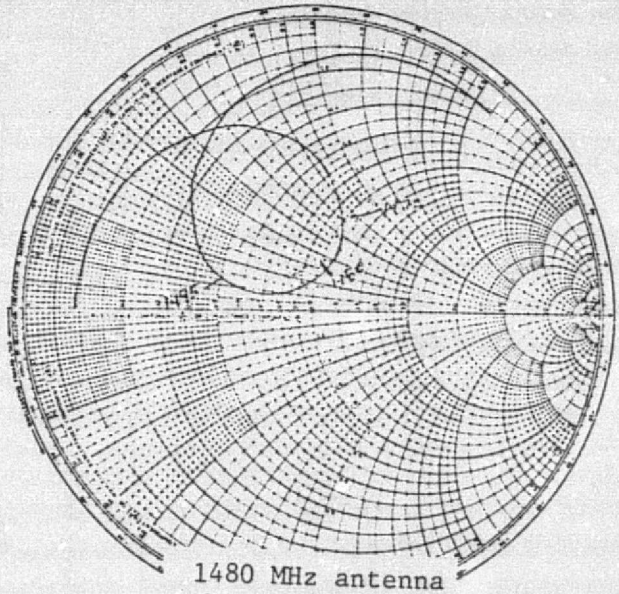

1480 MHz antenna

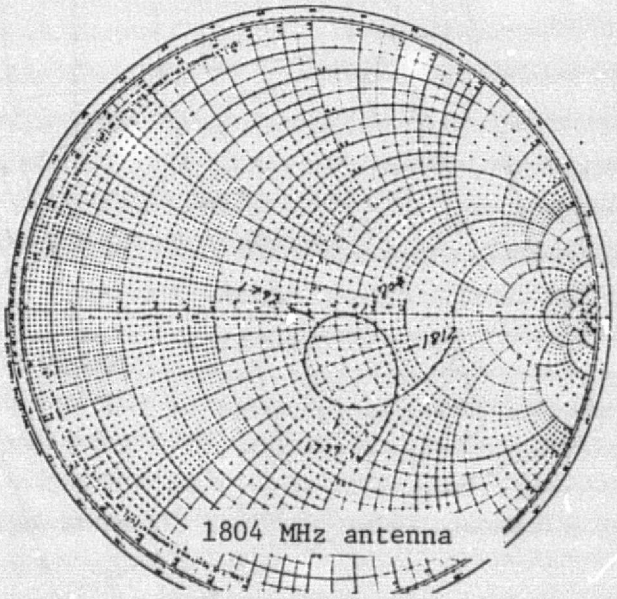

1804 MHz antenna

Figure 30. - Impedance characteristics of the L-band microstrip array for the Aircraft Drone.

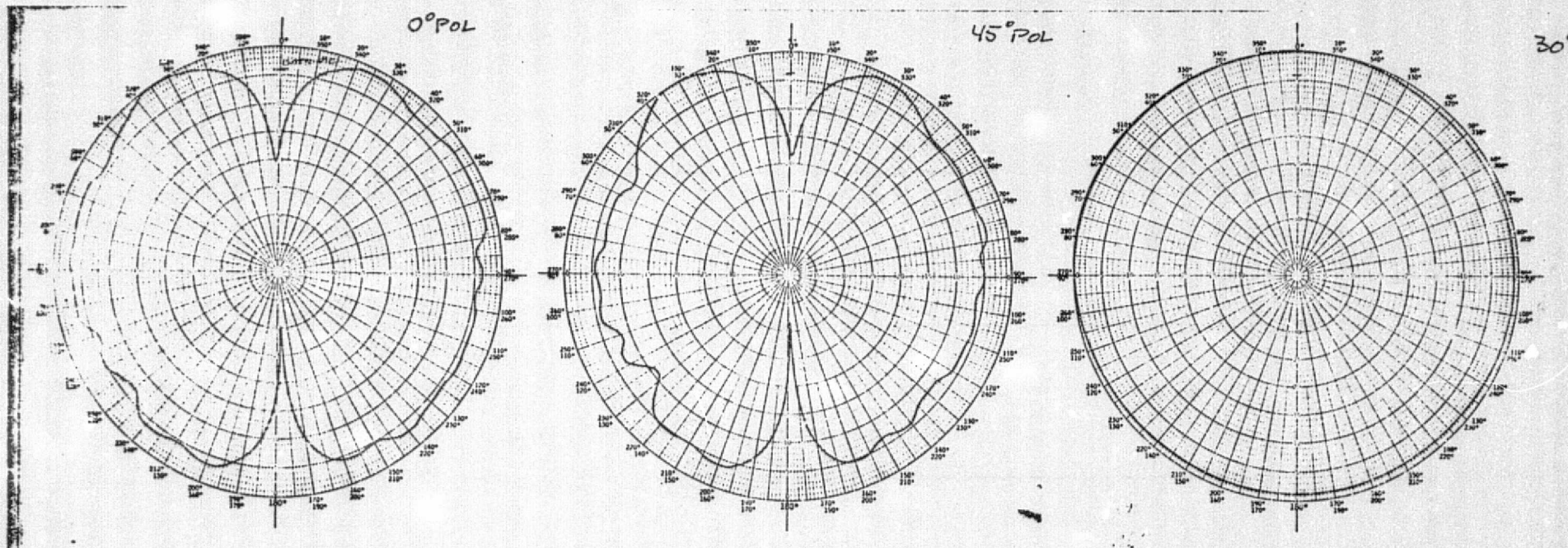

(a) Azimuthal plane pattern

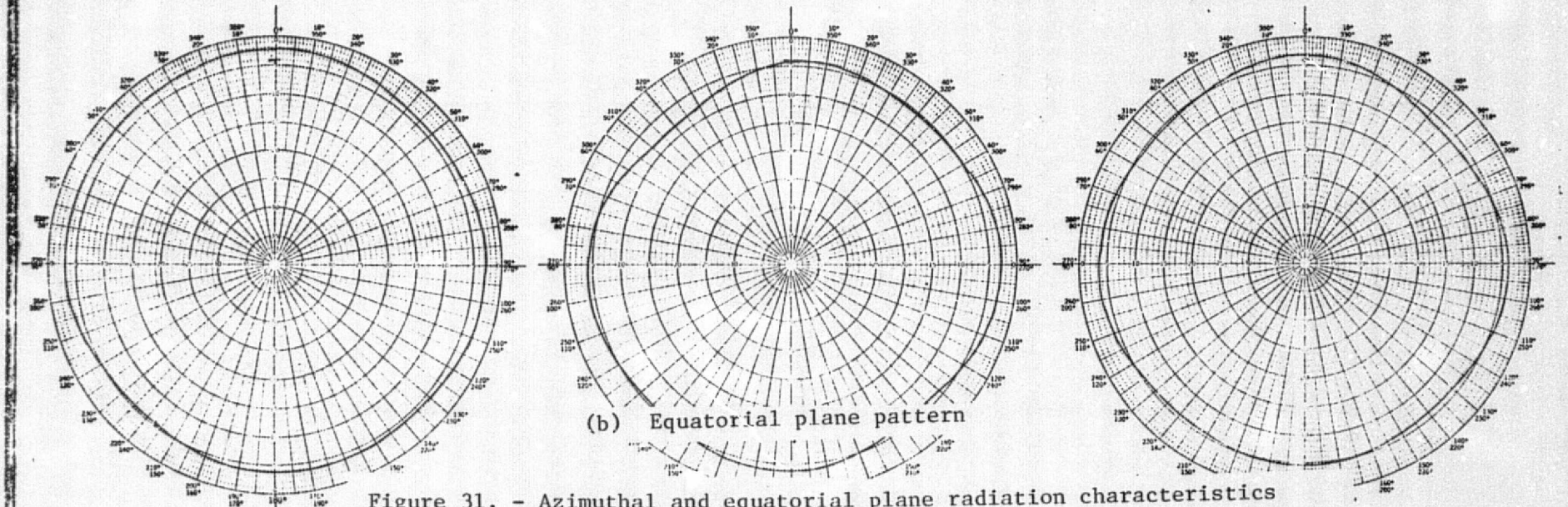

(b) Equatorial plane pattern

Figure 31. - Azimuthal and equatorial plane radiation characteristics for the L-band microstrip arrays for the